J|A|C|S
ARTICLES
Published on Web 01/19/2006

Solid-State $^{35/37}$Cl NMR Spectroscopy of Hydrochloride Salts of Amino Acids Implicated in Chloride Ion Transport Channel Selectivity: Opportunities at 900 MHz

David L. Bryce,* Gregory D. Sward, and Samyuktha Adiga

Contribution from the Department of Chemistry, University of Ottawa, Ottawa, Ontario K1N 6N5, Canada

Received October 24, 2005; E-mail: dbryce@uottawa.ca

Abstract: The results of a detailed systematic chlorine solid-state NMR study of several hydrochloride salts of amino acids implicated in chloride ion transport channel selectivity are reported. ^{35}Cl and ^{37}Cl NMR spectra have been obtained for stationary and/or magic-angle spinning powdered samples of the following compounds on 500 and/or 900 MHz spectrometers: DL-arginine HCl monohydrate, L-lysine HCl, L-serine HCl, L-glutamic acid HCl, L-proline HCl, L-isoleucine HCl, L-valine HCl, L-phenylalanine HCl, and glycine HCl. Spectral analyses provide information on the anisotropic properties and relative orientations of the chlorine electric field gradient and chemical shift (CS) tensors, which are intimately related to the local molecular and electronic structure. Data obtained at 900 MHz provide unique examples of the effects of CS anisotropy on the NMR spectrum of a quadrupolar nucleus. The range of chlorine quadrupolar coupling constants (C_Q) measured, −6.42 to 2.03 MHz, demonstrates the sensitivity of this parameter to the chloride ion environment and suggests the applicability of chlorine solid-state NMR as a novel experimental tool for defining chloride binding environments in larger ion channel systems. Salts of hydrophobic amino acids are observed to tend to exhibit larger values of C_Q than salts of hydrophilic amino acids. A simple model for rationalizing the observed trend in C_Q is proposed. For salts for which neutron diffraction structures are available, we identify a quantum chemical method which reproduces experimental values of C_Q with a root-mean-square deviation of 0.1 MHz and a correlation coefficient of 0.9998. On the basis of this, chlorine NMR tensors are predicted for the Cl^- binding site in ClC channels.

Introduction

Chloride ion channels are proteins which carry electric current across cell membranes and are essential for many biological processes.[1−3] Genetic defects related to chloride ion channels are known to cause serious health problems including cystic fibrosis, Bartter's syndrome, Dent's disease, and deafness. [4−11] The ClC Cl^- anion channels,[12−15] found in both eukaryotic and prokaryotic cells, have received much attention in recent years, most spectacularly in the form of X-ray crystal structures of two channels which were published in 2002 by MacKinnon and co-workers.[16] Subsequent studies by this group probed the structural basis of ClC channel selectivity and gating.[17]

Although X-ray crystallographic studies undoubtedly provide a wealth of information on biologically important molecules including anion transport channels,[16,17] cation transport channels,[18,19] enzymes,[20−25] and nucleic acids,[26,27] NMR spectroscopy

* To whom correspondence should be addressed. Phone: 613-562-5800 ext 2018. Fax: 613-562-5170.

(1) Guggino, W. B. In *Chloride Channels: Current Topics in Membranes*; Kleinzeller, A., Fambrough, D. M., Eds.; Academic Press: San Diego, 1994; Vol. 42.
(2) Ashcroft, F. M. *Ion Channels and Disease*; Academic Press: San Diego, 2000.
(3) Loewen, M. E.; Forsyth, G. W. *Physiol. Rev.* **2005**, *85*, 1061−1092.
(4) Ko, Y. H.; Pedersen, P. L. *J. Bioenerg. Biomembr.* **2001**, *33*, 513−521.
(5) Zhang, Z.-R.; Cui, G.; Liu, X.; Song, B.; Dawson, D. C.; McCarty, N. A. *J. Biol. Chem.* **2005**, *280*, 458−468.
(6) Riordan, J. R. et al. *Science* **1989**, *245*, 1066−1073.
(7) Simon, D. B. et al. *Nat. Genet.* **1997**, *17*, 171−178.
(8) Jentsch, T. J.; Maritzen, T.; Zdebik, A. A. *J. Clin. Invest.* **2005**, *115*, 2039−2046.
(9) Rowe, S. M.; Miller, S.; Sorscher, E. J. *N. Engl. J. Med.* **2005**, *352*, 1992−2001.
(10) Riordan, J. R. *Annu. Rev. Physiol.* **2005**, *67*, 701−718.
(11) Chen, T.-Y. *Annu. Rev. Physiol.* **2005**, *67*, 809−39.
(12) Jentsch, T. J.; Neagoe, I.; Scheel, O. *Curr. Opin. Neurobiol.* **2005**, *15*, 319−325.
(13) Jentsch, T. J.; Friedrich, T.; Schriever, A.; Yamada, H. *Pfluegers Arch.* **1999**, *437*, 783−795.
(14) Maduke, M.; Miller, C.; Mindell, J. A. *Annu. Rev. Biophys. Biomol. Struct.* **2000**, *29*, 411−438.
(15) Dutzler, R. *Trends Neurosci.* **2004**, *27*, 315−320.
(16) Dutzler, R.; Campbell, E. B.; Cadene, M.; Chait, B. T.; MacKinnon, R. *Nature* **2002**, *415*, 287−294.
(17) Dutzler, R.; Campbell, E. B.; MacKinnon, R. *Science* **2003**, *300*, 108−112.
(18) Long, S. B.; Campbell, E. B.; MacKinnon, R. *Science* **2005**, *309*, 897−903.
(19) Jiang, Y.; Lee, A.; Chen, J.; Ruta, V.; Cadene, M.; Chait, B. T.; MacKinnon, R. *Nature* **2003**, *423*, 33−41.
(20) Apiyo, D.; Zhao, L.; Tsai, M.-D.; Selby, T. L. *Biochemistry* **2005**, *44*, 9980−9989.
(21) Schubert, H. L.; Wilson, K. S.; Raux, E.; Woodcock, S. C.; Warren, M. J. *Nat. Struct. Biol.* **1998**, *5*, 585−592.
(22) Westover, K. D.; Bushnell, D. A.; Kornberg, R. D. *Science* **2004**, *303*, 1014−1016.
(23) Bushnell, D. A.; Westover, K. D.; Davis, R. E.; Kornberg, R. D. *Science* **2004**, *303*, 983−988.
(24) Cramer, P.; Bushnell, D. A.; Kornberg, R. D. *Science* **2001**, *292*, 1863−1876.
(25) Gnatt, A. L.; Cramer, P.; Fu, J.; Bushnell, D. A.; Kornberg, R. D. *Science* **2001**, *292*, 1876−1882.
(26) Shi, H.; Moore, P. B. *RNA* **2000**, *6*, 1091−1105.
(27) Egli, M. *Curr. Opin. Chem. Biol.* **2004**, *8*, 580−591.

offers a unique and important perspective in the determination of biomolecular structure and dynamics in solution[28−32] and, increasingly, in the solid state.[33−44] The emphasis of these studies is largely on the determination of the structure of the protein or nucleic acid backbone and, in some cases, amino acid side chains. Effort has also been devoted to studying directly, by solid-state NMR (SSNMR) spectroscopy, metal cations in various biologically relevant systems.[45,46] For example, Wu and co-workers have applied ^{23}Na SSNMR to study the sodium cation environment in a guanine quadruplex formed by the *Oxytricha nova* telomere repeat d($G_4T_4G_4$)[47] as well as a G-quartet structure formed by guanosine 5′-monophosphate.[48] Lipton, Ellis, and co-workers have applied ^{67}Zn SSNMR at high magnetic fields and low temperature to characterize the zinc binding environment in carbonic anhydrase, a DNA binding domain of the human nucleotide excision repair protein XPA, and related model systems.[49−52] It is clearly of interest to explore the development of methods which are complementary to X-ray crystallography for characterizing and studying the binding sites in chloride anion transport channels.

We have recently reviewed[53] the literature involving SSNMR studies of $^{35/37}$Cl, $^{79/81}$Br, and ^{127}I isotopes, and it is apparent that although this field of research is underdeveloped it holds great promise for studying diverse chemical and biochemical systems. Previous limited $^{35/37}$Cl studies of chloride anions in organic hydrochloride salts portend that chlorine SSNMR may exhibit potential for the characterization of chloride anion binding sites in ion channels and related model systems.[54−57]

Chart 1. Nominal Structures of the Amino Acid Cation Portions of the Amino Acid Hydrochloride Salts Studied

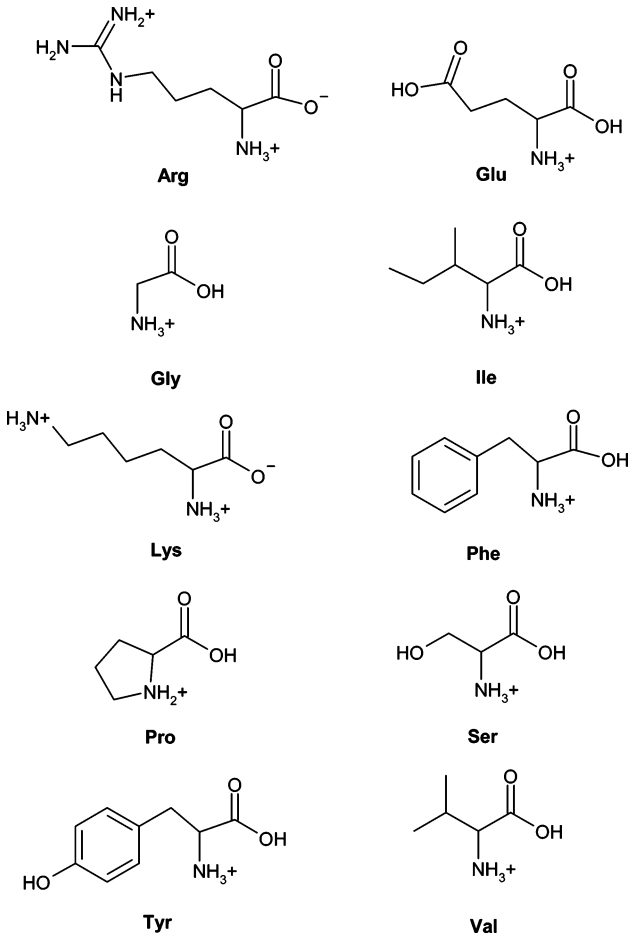

On the basis of data available at the time, a model for rationalizing the trend in chlorine quadrupolar coupling constants for organic hydrochloride salts has been proposed.[54]

To establish a firm basis on which experimental protocols and theoretical interpretations may be developed for application to studies of intact ion channels, it is imperative to perform a systematic study of smaller model systems with this goal in mind. In the present work, we establish and demonstrate the utility of chlorine-35/37 SSNMR spectroscopy in acting as a useful probe of the chloride ion binding environment in amino acid hydrochlorides, which are representative of the chloride ion binding environment in the ClC ion channels. The ion binding site in ClC channels includes the highly conserved amino acid sequences Gly-Ser-Gly-Ile-Pro, Gly-(Lys/Arg)-Glu-Gly-Pro, and Gly-X-Phe-X-Pro.[16] Arginine is also known to be a key residue in the activation of cardiac pacemaker chloride ion channels.[58] Interactions of chloride with phenylalanine are also of interest because the most common cause of cystic fibrosis is the deletion of a phenylalanine residue at position 508 in the cystic fibrosis transmembrane conductance regulator (CFTR) chloride ion channel.[59,60] The amino acid cation portions of the hydrochloride salts studied in the present work are shown in Chart 1.

(28) Bax, A. *Protein Sci.* **2003**, *12*, 1−16.
(29) Bax, A.; Kontaxis, G.; Tjandra, N. *Methods Enzymol. Part B* **2001**, *339*, 127−174.
(30) Hwang, P. M.; Kay L. E. *Methods Enzymol., Part C* **2005**, *394*, 335−350.
(31) Kay, L. E. *J. Magn. Reson.* **2005**, *173*, 193−207.
(32) Wüthrich, K. *Angew. Chem., Int. Ed.* **2003**, *42*, 3340−3363.
(33) Marulanda, D.; Tasayco, M. L.; McDermott, A.; Cataldi, M.; Arriaran, V.; Polenova, T. *J. Am. Chem. Soc.* **2004**, *126*, 16608−16620.
(34) Zech, S. G.; Wand, A. J.; McDermott, A. E. *J. Am. Chem. Soc.* **2005**, *127*, 8618−8626.
(35) McDermott, A. E. *Curr. Opin. Struct. Biol.* **2004**, *14*, 554−561.
(36) Paulson, E. K.; Morcombe, C. R.; Gaponenko, V.; Dancheck, B.; Byrd, R. A.; Zilm, K. W. *J. Am. Chem. Soc.* **2003**, *125*, 14222−14223.
(37) Luca, S.; Heise, H.; Baldus, M. *Acc. Chem. Res.* **2003**, *36*, 858−865.
(38) Lange, A.; Becker, S.; Seidel, K.; Giller, K.; Pongs, O.; Baldus, M. *Angew. Chem., Int. Ed.* **2005**, *44*, 2089−2092.
(39) Siemer, A. B.; Ritter, C.; Ernst, M.; Riek, R.; Meier, B. H. *Angew. Chem., Int. Ed.* **2005**, *44*, 2441−2444.
(40) Jaroniec, C. P.; MacPhee, C. E.; Bajaj, V. S.; McMahon, M. T.; Dobson, C. M.; Griffin, R. G. *Proc. Natl. Acad. Sci. U.S.A.* **2004**, *101*, 711−716.
(41) Franks, W. T.; Zhou, D. H.; Wylie, B. J.; Money, B. G.; Graesser, D. T.; Frericks, H. L.; Sahota, G.; Rienstra, C. M. *J. Am. Chem. Soc.* **2005**, *127*, 12291−12305.
(42) Williamson, P. T. F.; Meier, B. H.; Watts, A. *Eur. Biophys. J.* **2004**, *33*, 247−254.
(43) Sharpe, S.; Kessler, N.; Anglister, J. A.; Yau, W.-M.; Tycko, R. *J. Am. Chem. Soc.* **2004**, *126*, 4979−4990.
(44) Chan, J. C. C.; Oyler, N. A.; Yau, W.-M.; Tycko, R. *Biochemistry* **2005**, *44*, 10669−10680.
(45) Power, W. P.; Kirby, C. W.; Taylor, N. J. *J. Am. Chem. Soc.* **1998**, *120*, 9428−9434.
(46) Wu, G. *Biochem. Cell. Biol.* **1998**, *76*, 429−442.
(47) Wu, G.; Wong, A. *Biochem. Biophys. Res. Commun.* **2004**, *323*, 1139−1144.
(48) Wong, A.; Wu, G. *J. Am. Chem. Soc.* **2003**, *125*, 13895−13905.
(49) Lipton, A. S.; Heck, R. W.; Ellis, P. D. *J. Am. Chem. Soc.* **2004**, *126*, 4735−4739.
(50) Lipton, A. S.; Bergquist, C.; Parkin, G.; Ellis, P. D. *J. Am. Chem. Soc.* **2003**, *125*, 3768−3772.
(51) Lipton, A. S.; Wright, T. A.; Bowman, M. K.; Reger, D. L.; Ellis, P. D. *J. Am. Chem. Soc.* **2002**, *124*, 5850−5860.
(52) Lipton, A. S.; Buchko, G. W.; Sears, J. A.; Kennedy, M. A.; Ellis, P. D. *J. Am. Chem. Soc.* **2001**, *123*, 992−993.
(53) Bryce, D. L.; Sward, G. D. *Magn. Reson. Chem.*, in press.
(54) Bryce, D. L.; Gee, M.; Wasylishen, R. E. *J. Phys. Chem. A* **2001**, *105*, 10413−10421.
(55) Gervais, C.; Dupree, R.; Pike, K. J.; Bonhomme, C.; Profeta, M.; Pickard, C. J.; Mauri, F. *J. Phys. Chem. A* **2005**, *109*, 6960−6969.
(56) Honda, H. *Z. Naturforsch.* **2003**, *58a*, 623−630.
(57) Hattori, M.; Onoda, Y.; Erata, T.; Smith, M. E.; Hattori, M.; Ohki, H.; Ikeda, R. *Z. Naturforsch.* **1994**, *49a*, 291−296.
(58) Wahl-Schott, C.; Baumann, L.; Zong, X.; Biel, M. *J. Biol. Chem.* **2005**, *280*, 13694−13700.
(59) Cheng, S. H.; Gregory, R. J.; Marshall, J.; Paul, S.; Souza, D. W.; White, G. A.; O'Riordan, C. R.; Smith, A. E. *Cell* **1990**, *63*, 827−834.

Chlorine-35 (natural abundance (NA) = 75.53%) and chlorine-37 (NA = 24.47%) are both quadrupolar nuclei with nuclear spins of 3/2. This fact complicates spectral acquisition and interpretation but by the same token offers a wealth of information which is unavailable from solution NMR studies or X-ray crystallographic studies. In particular, under favorable circumstances, information is available on the orientation-dependent electric field gradient (EFG) and chemical shift (CS) tensors of the chlorine nucleus. These second-rank tensors are intimately dependent on the local molecular (e.g., hydrogen-bonding environment) and electronic structure. Ultrahigh-field NMR spectrometers, such as the 900 MHz instrument at the National Ultrahigh-Field NMR Facility for Solids in Ottawa, Canada, offer new opportunities for the study of challenging quadrupolar nuclei including $^{35/37}$Cl. Specifically, high magnetic fields (B_0) are advantageous for quadrupolar nuclei for two primary reasons in addition to the increase in the signal-to-noise ratio experienced by all nuclei: (i) the inverse scaling of the breadth of the second-order quadrupolar powder pattern with B_0 means that narrower lines are obtained at higher fields and (ii) the chemical shift interaction increases linearly with B_0 (in Hz), thereby creating new opportunities for the measurement of complete CS tensor properties. Interpretation of the experimental data in concert with high-level quantum chemical calculations has the potential to offer valuable insights into the relationship between the NMR data and the structural properties of various chloride ion binding sites.

Theoretical Background

Because ^{35}Cl and ^{37}Cl both have nuclear spin quantum numbers of 3/2, their NMR spectra will be affected by the nuclear quadrupolar interaction between their nuclear quadrupole moment (Q) and the surrounding EFG, in addition to the nuclear magnetic shielding (σ) interaction. The Hamiltonian operator for ^{35}Cl or ^{37}Cl in a magnetic field may therefore be written in a general form as:

$$\hat{H} = \hat{H}_Z + \hat{H}_Q + \hat{H}_\sigma \tag{1}$$

where the first term represents the Zeeman interaction, the second represents the quadrupolar interaction, and the third represents the magnetic shielding interaction. In the present work, we observe only the central transition (CT, $1/2 \leftrightarrow -1/2$). The satellite transitions (ST, $\pm 3/2 \leftrightarrow \pm 1/2$) are much broader than the CT and are thus more difficult to observe. Use is made in this work of the ST populations for signal enhancement purposes according to the hyperbolic secant spin−echo sequence of Siegel et al.[61,62]

Nuclear Magnetic Shielding and Chemical Shift Tensors. The Zeeman and magnetic shielding Hamiltonians may be combined and written as:

$$\hat{H}_{Z,\sigma} = -\frac{\gamma h}{2\pi}(\hat{\mathbf{I}}(\mathbf{1} - \boldsymbol{\sigma})B_0) \tag{2}$$

where $\hat{\mathbf{I}}$ is the nuclear spin angular momentum operator, $\mathbf{1}$ is the unit tensor, $\boldsymbol{\sigma}$ is the nuclear magnetic shielding tensor, and B_0 is the applied magnetic field. According to Ramsey's theory, $\boldsymbol{\sigma}$ may be expressed as a sum of diamagnetic and paramagnetic terms.[63−67]

The $\boldsymbol{\sigma}$ tensor is a general second-rank tensor which may be decomposed into isotropic (σ_{iso}), symmetric (σ_{sym}), and antisymmetric parts ($\sigma_{antisym}$). The antisymmetric part[68] is very difficult to characterize and does not influence the appearance of NMR spectra to first order; we ignore its influence in the present work. The sum of the symmetric and isotropic parts of $\boldsymbol{\sigma}$ consists of up to six independent components. In its principal axis system (PAS), $\sigma_{iso} + \sigma_{sym}$ is diagonal and is characterized by three eigenvalues labeled and ordered as $\sigma_{33} \geq \sigma_{22} \geq \sigma_{11}$, three eigenvectors which define the orientation of the PAS relative to an external axis system, and the isotropic shielding constant which is equal to the average of the three eigenvalues, $\sigma_{iso} = (\sigma_{11} + \sigma_{22} + \sigma_{33})/3$. As can been seen from eq 2, the effects of an anisotropic nuclear magnetic shielding tensor on the NMR spectrum scale linearly with the strength of the applied magnetic field.

In an NMR experiment, chemical shifts (δ) are measured rather than magnetic shielding constants. For example, the isotropic chemical shift is related to the magnetic shielding constant as shown:

$$\delta_{iso} = \frac{\sigma_{iso}(\text{ref}) - \sigma_{iso}}{1 - \sigma_{iso}(\text{ref})} \approx \sigma_{iso}(\text{ref}) - \sigma_{iso} \tag{3}$$

where the second equality is valid for most light elements because shielding constants are on the order of 10^{-6} (often expressed as parts per million). An analogous equation may be used to convert the eigenvalues of the shielding tensor to those of the CS tensor ($\delta_{11} \geq \delta_{22} \geq \delta_{33}$).

Quantum chemistry provides magnetic shielding tensors rather than chemical shift tensors. To compare experiment and theory, the value of σ_{iso}(ref) must be known. Conversion of chlorine shielding constants to chemical shifts may be achieved using the chlorine absolute shielding scale of Gee et al.:[69]

$$\delta = 974 \text{ ppm} - \sigma \tag{4}$$

which is correct for an infinitely dilute aqueous NaCl solution.

Although the three eigenvalues convey all the information about the magnitude of the shielding or CS tensor, the span (Ω) and skew (κ) are alternative convenient representations of the breadth and asymmetry of the $\boldsymbol{\sigma}$ and $\boldsymbol{\delta}$ tensors:[70]

$$\Omega = \sigma_{33} - \sigma_{11} \approx \delta_{11} - \delta_{33} \tag{5}$$

$$\kappa = \frac{3(\sigma_{iso} - \sigma_{22})}{\Omega} \approx \frac{3(\delta_{22} - \delta_{iso})}{\Omega} \tag{6}$$

Nuclear Electric Quadrupolar Interaction. The second term in eq 1 represents the interaction between the second-rank EFG

(60) Kerem, B.; Rommens, J. M.; Buchanan, J. A.; Markiewicz, D.; Cox, T. K.; Chakravarti, A.; Buchwald, M.; Tsui, L.-C. *Science* **1989**, *245*, 1073−1080.
(61) Siegel, R.; Nakashima, T. T.; Wasylishen, R. E. *Chem. Phys. Lett.* **2004**, *388*, 441−445.
(62) Siegel, R.; Nakashima, T. T.; Wasylishen, R. E. *Concepts Magn. Reson. Part A* **2005**, *26A*, 47−61.
(63) Ramsey, N. F. *Molecular Beams*; Oxford University Press: London, 1956; pp 162−166, 208−213.
(64) Ramsey, N. F. *Phys. Rev.* **1950**, *77*, 567.
(65) Ramsey, N. F. *Phys. Rev.* **1950**, *78*, 699−703.
(66) Ramsey, N. F. *Phys. Rev.* **1951**, *83*, 540−541.
(67) Ramsey, N. F. *Phys. Rev.* **1952**, *86*, 243−246.
(68) Wi, S.; Frydman, L. *J. Chem. Phys.* **2002**, *116*, 1551−1561.
(69) Gee, M.; Wasylishen, R. E.; Laaksonen, A. *J. Phys. Chem. A* **1999**, *103*, 10805−10812.
(70) Mason, J. *Solid State Nucl. Magn. Reson*. **1993**, *2*, 285−288.

tensor and the nuclear electric quadrupole moment. The tensor is traceless, does not have an antisymmetric component, and may be diagonalized to yield three eigenvectors and eigenvalues. The eigenvalues of the EFG tensor are labeled and ordered as follows: $|V_{33}| \geq |V_{22}| \geq |V_{11}|$. Quadrupolar coupling constants may be obtained according to the following equation:

$$C_{\mathrm{Q}} = \frac{eV_{33}\mathrm{Q}}{h} \tag{7}$$

Here, e is the charge on an electron, h is Planck's constant, and Q is the nuclear electric quadrupole moment. The asymmetry parameter of the EFG tensor is defined as:

$$\eta_{\mathrm{Q}} = \frac{V_{11} - V_{22}}{V_{33}} \tag{8}$$

In the high-field approximation, where the Larmor frequency (ν_{L}) is much greater than the quadrupolar frequency, $\nu_{\mathrm{Q}} = 3C_{\mathrm{Q}}/((2I(2I-1))$, the quadrupolar Hamiltonian is given to first order as

$$\hat{H}_{\mathrm{Q}} = h\frac{C_{\mathrm{Q}}}{8I(2I-1)}(3\hat{I}_z^{\,2} - \hat{I}^2)(3\cos^2\theta - 1 + \eta_{\mathrm{Q}}\sin^2\theta\cos 2\phi) \tag{9}$$

where θ and ϕ are polar angles which define the orientation of B_0 in the PAS of the EFG tensor. It is important to note that the second-order quadrupolar effects observed in the present study arise from a quadrupolar cross term which gives rise to a fourth-rank tensor.[71]

The breadth of the CT NMR line shape in a stationary powdered sample due to the quadrupolar interaction is given by:[72]

$$\Delta\nu_{\mathrm{CT}} = \frac{(25 + 22\eta_{\mathrm{Q}} + \eta_{\mathrm{Q}}^{\,2})}{144}\left[\frac{(3C_{\mathrm{Q}})^2}{((2I)(2I-1))^2}\right]\left[\frac{I(I+1) - \frac{3}{4}}{\nu_{\mathrm{L}}}\right] \tag{10}$$

Here, it is seen that the breadth scales inversely with the applied magnetic field. When the static line width is narrow enough, MAS experiments are useful in further narrowing of the CT line width by a factor of 3 to 4.[73−75]

Relative Tensor Orientations. Under favorable circumstances, NMR spectra of powdered samples of quadrupolar nuclei are amenable to a complete analysis which yields the magnitudes of both the EFG and the CS tensors as well as their relative orientations.[76,77] Three Euler angles (α, β, and γ) are required to completely describe how the two PASs are related. The angles define the counterclockwise rotations required to bring the EFG PAS into coincidence with the CS PAS. The "$z-y-z$" Arfken convention[78] is used in the present work, where α describes the initial counterclockwise rotation about the z-axis of the coordinate system, β is the subsequent rotation about the y-axis of the new coordinate system, and γ is the final rotation about the new z-axis.

Experimental and Computational Details

(i) Sample Preparation and Characterization. DL-Arginine hydrochloride monohydrate, L-glutamic acid, and glycine hydrochloride were purchased from Aldrich. All other amino acid hydrochlorides (L-valine HCl, L-phenylalanine HCl, L-proline HCl, L-isoleucine HCl, L-serine HCl, and L-lysine HCl) were prepared by dissolving the corresponding amino acid (obtained from Aldrich) in dilute hydrochloric acid, which was brought to a gentle boil. After cooling, the hydrochloride salts slowly crystallized from the solution and were filtered. Phase purity of selected salts was confirmed by ^{13}C cross-polarization magic-angle spinning (CP/MAS) NMR spectroscopy at 4.7 T.

Melting points were obtained for selected hydrochloride salts using a Barnstead/Electrothermal Mel-Temp melting point apparatus: 170−172 °C (glycine HCl); 128−130 °C (DL-arginine HCl monohydrate); 206−208 °C, dec (L-phenylalanine HCl); 140−148 °C (L-serine HCl); 195−197 °C (L-glutamic acid HCl); 242−249 °C, dec (L-lysine HCl); 204−209 °C (L-isoleucine HCl).

Special care was taken in dealing with samples of glycine HCl and L-proline HCl, which are hygroscopic (particularly L-Pro HCl). Prior to packing samples of these compounds, they were dried in vacuo for several hours to remove excess water. A narrow ^{35}Cl NMR resonance due to solvated molecules was observed for some samples (e.g., isoleucine HCl, phenylalanine HCl, and glycine HCl). However, the CT powder pattern observed after dehydration of the samples was identical to that observed before dehydration, consistent with the notion that no change to the solid-state structure occurred as a result of placing the samples in vacuo.

(ii) Solid-State NMR Spectroscopy. (a) 500 MHz Data. Samples were powdered and packed into 4.0 mm o.d. zirconia rotors, and NMR experiments were carried out at 11.75 T (500 MHz ^{1}H frequency) using a Bruker Avance spectrometer and XWinNMR 3.2 software. A Bruker 4.0 mm HX double-resonance MAS probe tuned to ^{35}Cl (49.00 MHz) or ^{37}Cl (40.79 MHz) on the X channel was used. The magic angle was set by maximizing the number of rotational echoes in the ^{79}Br FID of solid KBr while spinning at 5 kHz.[79] Experimental setup, referencing, and pulse calibration were performed using solid sodium chloride, for which the intense centerband was set to 0 ppm. Typical "solution $\pi/2$" pulse lengths were 4.3−4.4 μs. The "solid $\pi/2$" used was therefore, e.g., 4.36 μs/$(I + {}^1/_2) = 2.18$ μs. Quadrupolar echo sequences were used in all cases, for both MAS and stationary samples. Recycle delays were typically 0.5−2.0 s, and signal averaging was carried out over a period ranging from 1 h for MAS samples to 16 h for some stationary samples. Proton decoupling was applied during acquisition; however, for stationary samples, this had little noticeable effect. In addition to a $\pi/2 - \tau - \pi - \tau -$ ACQ echo pulse sequence, the double hyperbolic secant echo sequence of Siegel et al.[61,62] was also employed to provide signal enhancements. For this latter pulse sequence, the hyperbolic secant pulses for inversion of the satellite transition populations were typically offset at ±650 kHz and had a typical duration of 3000 μs.

(b) 900 MHz Data. Samples were powdered and packed into 5.0 mm glass tubes, which were inserted into a home-built (J. Bennett, National Research Council, Ottawa) single-channel solenoid probe tuned to ^{35}Cl (88.13 MHz) or ^{37}Cl (73.36 MHz). Experiments were performed using a standard-bore 21.15 T magnet (900 MHz ^{1}H frequency) and a Bruker Avance II console running TopSpin software at the National Ultrahigh-Field NMR Facility for Solids in Ottawa

(71) Frydman, L. *Annu. Rev. Phys. Chem.* **2001**, *52*, 463−498.
(72) Amoureux, J. P.; Fernandez, C.; Granger, P. In *Multinuclear Magnetic Resonance in Liquids and Solids − Chemical Applications*; Granger, P., Harris, R. K., Eds.; NATO ASI Series C; Kluwer Academic Publishers: Dordrecht, 1990; Chapter XXII, Vol. 322.
(73) Kundla, E.; Samoson, A.; Lippmaa, E. *Chem. Phys. Lett.* **1981**, *83*, 229−232.
(74) Samoson, A.; Kundla, E.; Lippmaa, E. *J. Magn. Reson.* **1982**, *49*, 350−357.
(75) Behrens, H. J.; Schnabel, B. *Physica* **1982**, *114B*, 185−190.
(76) Power, W. P.; Wasylishen, R. E.; Mooibroek, S.; Pettitt, B. A.; Danchura, W. *J. Phys. Chem.* **1990**, *94*, 591−598.
(77) Chu, P. J.; Gerstein, B. C. *J. Chem. Phys.* **1989**, *91*, 2081−2101.
(78) Arfken, G. B. *Mathematical Methods for Physicists*; Academic Press: New York, 1985.
(79) Frye, J. S.; Maciel, G. E. *J. Magn. Reson.* **1982**, *48*, 125−131.

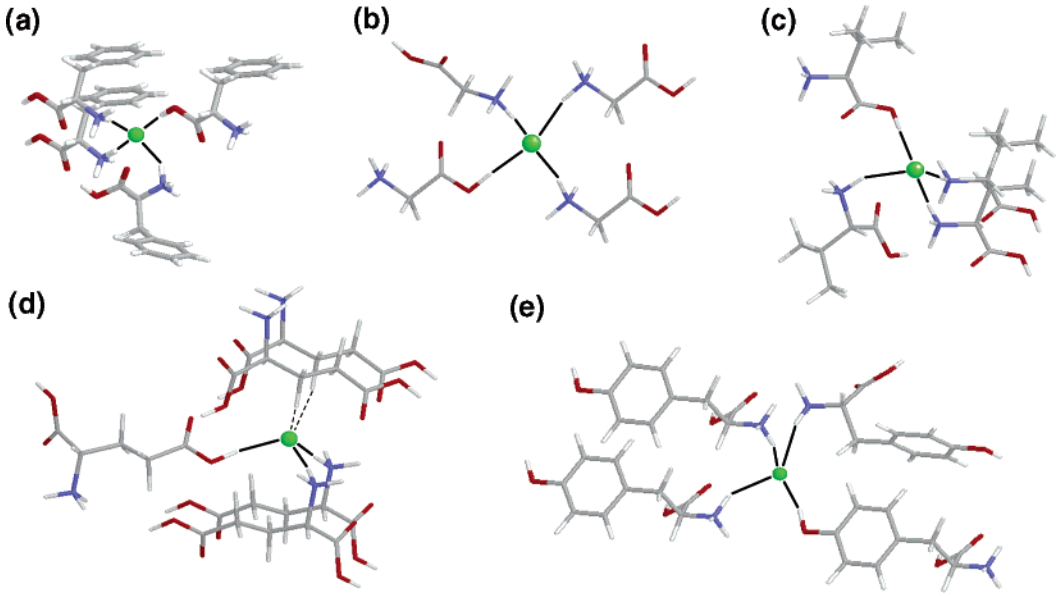

Figure 1. Coordination environment of the chloride ion (in green) in solid (a) L-phenylalanine hydrochloride, (b) glycine hydrochloride, (c) L-valine hydrochloride, (d) L-glutamic acid hydrochloride, and (e) L-tyrosine hydrochloride. Atomic coordinates are taken from neutron diffraction studies (see text). Hydrogen bonds to chlorine are indicated with black lines. In the case of L-Glu HCl, the inclusion of two additional glutamic acid moieties with methylene protons within 3.0 and 3.1 Å of the chloride ion (see dashed black lines) were essential in achieving calculated quadrupolar coupling constants in agreement with experiment.

(http://www.nmr900.ca). Experimental setup, referencing, and pulse calibration were performed using an aqueous sodium chloride solution. For ^{35}Cl, the solution $\pi/2$ pulse width was calibrated as 6.0 μs and the solid $\pi/2$ used was therefore 3.0 μs. For ^{37}Cl, the calibrated solid $\pi/2$ pulse was 4.0 μs. A simple single-pulse sequence was used to acquire the spectra. The probe dead time was approximately 10 μs. Recycle delays were 0.5−2.0 s, and signal averaging was typically carried out over a period ranging from 1 to 3 h.

(c) Spectral Processing and Simulation. Data were processed using Bruker's XWinNMR software (version 3.2) or TopSpin software. FIDs were left-shifted where necessary, apodized using a Gaussian function of <100 Hz for MAS samples or 100−2000 Hz for stationary samples, zero-filled to at least twice their original size, and Fourier transformed. Phase corrections and cubic spline baseline corrections were applied for one-pulse spectra acquired at 21.15 T. Stack plots were prepared using DMFit.[80] Spectral simulations were performed using the WSOLIDS1 program,[81] which incorporates the space-tiling algorithm of Alderman et al.[82] Some MAS spectra were simulated using SIMPSON.[83] All spectra were interpreted within the high-field approximation; the largest ^{35}Cl quadrupole frequency measured (3.21 MHz, vide infra) represents only 6.6% of the ^{35}Cl Larmor frequency in the lowest magnetic field used ($B_0 = 11.75$ T; $\nu_L = 49.0$ MHz). All spectra were simulated on the basis of a single magnetically unique chlorine site. Special emphasis was placed on fitting the spectral discontinuities and shoulders along the frequency dimension as opposed to spectral intensities across the powder patterns because it is well-known that nonuniform excitation may adversely affect these spectral intensities.

(iii) Quantum Chemical Calculations. EFG and $\boldsymbol{\sigma}$ tensors were calculated using Gaussian 03.[84] Calculations were performed using atomic coordinates from the neutron diffraction studies of Al-Karaghouli and Koetzle[85] for L-phenylalanine hydrochloride, Koetzle et al.[86] for L-valine hydrochloride, Frey et al.[87] for L-tyrosine hydrochloride, Sequeira et al.[88] for L-glutamic acid hydrochloride, and Al-Karaghouli et al.[89] for glycine hydrochloride. No quantum chemical geometry minimization was performed on the structures. A crystal lattice extending over several unit cells in three dimensions was constructed for each amino acid hydrochloride with the available neutron diffraction coordinates, space group, and unit cell parameters using the program Diamond (version 3.0e).[90] From this lattice, a single chloride ion and its surrounding hydrogen-bonded amino acid cations were selected as appropriate models (Figure 1) for quantum chemical calculations.

A model for the chloride ion binding site in ClC ion channels was built using atomic coordinates available from X-ray crystallography (PDB entry 1KPL).[16] The model consisted of a single Cl^- and the following residues: Gly106, Ser107, Gly108, Ile109, Pro110, Gly355, Ile356, Phe357, Ala358, Glu148, Gly149, and Tyr445. Some side chains at the periphery of the model, which do not interact with Cl, were removed to reduce the computational time required. Dangling bonds were terminated with protons as appropriate. Proton positions were optimized at the B3LYP/3-21G* level; the heavy-atom positions were kept frozen during this optimization.

Restricted Hartree−Fock (RHF) calculations, as well as density-functional theory (DFT) calculations employing the hybrid B3LYP functional[91] or the PBE exchange and correlation functionals,[92] were carried out with a variety of Pople-type basis sets and Dunning-type (cc-pVDZ; aug-cc-pVDZ; cc-pVTZ)[93,94] basis sets which were available within the G03 package. Locally dense basis sets[95,96] were employed

(80) Massiot, D.; Fayon, F.; Capron, M.; King, I.; Le Calvé, S.; Alonso, B.; Durand, J.-O.; Bujoli, B.; Gan, Z.; Hoatson, G. *Magn. Reson. Chem.* **2002**, *40*, 70−76.
(81) Eichele, K.; Wasylishen R. E. *WSOLIDS NMR Simulation Package*, version 1.17.30; Dalhousie University: Halifax, 2001.
(82) Alderman, D. W.; Solum, M. S.; Grant, D. M. *J. Chem. Phys.* **1986**, *84*, 3717−3725.
(83) Bak, M.; Rasmussen, J. T.; Nielsen, N. C. *J. Magn. Reson.* **2000**, *147*, 296−330.
(84) Frisch, M. J. et al. *Gaussian 03*, revisions B.04 and C.02; Gaussian, Inc.: Wallingford, CT, 2004.
(85) Al-Karaghouli, A. R.; Koetzle, T. F. *Acta Crystallogr.* **1975**, *B31*, 2461−2465.
(86) Koetzle, T. F.; Golic, L.; Lehmann, M. S.; Verbist, J. J.; Hamilton, W. C. *J. Chem. Phys.* **1974**, *60*, 4690−4696.
(87) Frey, M. N.; Koetzle, T. F.; Lehmann, M. S.; Hamilton, W. C. *J. Chem. Phys.* **1973**, *58*, 2547−2556.
(88) Sequeira, A.; Rajagopal, H.; Chidambaram, R. *Acta Crystallogr.* **1972**, *B28*, 2514−2519.
(89) Al-Karaghouli, A. R.; Cole, F. E.; Lehmann, M. S.; Miskell, C. F.; Verbist, J. J.; Koetzle, T. F. *J. Chem. Phys.* **1975**, *63*, 1360−1366.
(90) Brandenburg, K. *Diamond*, version 3.0e, Crystal Impact GbR: Bonn, Germany, 1997−2005.
(91) Becke, A. D. *J. Chem. Phys.* **1993**, *98*, 5648−5652.
(92) (a) Perdew, J. P.; Burke, K.; Ernzerhof, M. *Phys. Rev. Lett.* **1996**, *77*, 3865−3868. (b) Perdew, J. P.; Burke, K.; Ernzerhof, M. *Phys. Rev. Lett.* **1997**, *78*, 1396.

Table 1. Chlorine-35/37 Solid-State NMR Data for Amino Acid Hydrochlorides: Electric Field Gradient and Chemical Shift Tensors

compound	$\lvert C_Q(^{35}Cl)\rvert$/MHz[a]	η_Q	δ_{iso}/ppm[b]	Ω/ppm	κ	α, β, γ[c]	ref
DL-arginine HCl monohydrate	2.03 ± 0.01	0.98 ± 0.02	91.5 ± 1.0	<150	[d]	[d]	this work
L-tyrosine HCl	(+)2.23 ± 0.02	0.72 ± 0.03	94.7 ± 0.5	<150	[d]	[d]	Bryce et al.[54]
L-tyrosine HCl	2.3 ± 0.1	0.7 ± 0.1	95 ± 1	[d]	[d]	[d]	Gervais et al.[55]
L-lysine HCl	2.49 ± 0.01	0.42 ± 0.02	105 ± 2	26 ± 10	−0.4 ± 0.4	0, 52, 0°	this work
L-serine HCl[e]	3.0 ± 0.3	0.8 ± 0.2	120 ± 30	<150	[d]	[d]	this work
L-glutamic acid HCl	(+)3.61 ± 0.01	0.65 ± 0.02	102 ± 1	66 ± 15	0.0 ± 0.3	9, 77, 6°	this work
L-glutamic acid HCl	3.7 ± 0.1	0.6 ± 0.1	104 ± 1	[d]	[d]	[d]	Gervais et al.[55]
L-proline HCl	(+)4.50 ± 0.05	0.63 ± 0.05	37 ± 5	63 ± 5	−0.54 ± 0.08	48, 69, 9°	this work
L-isoleucine HCl	4.39 ± 0.05	0.25 ± 0.03	96 ± 20	75 ± 30	>0.85	20, 12, 0°	this work
L-valine HCl[f]	(−)5.89 ± 0.05	0.51 ± 0.05	90 ± 10	125 ± 40	0.35 ± 0.50	65, 0, 0°	this work
L-valine HCl	6.0 ± 0.1	0.5 ± 0.1	114 ± 1	[d]	[d]	[d]	Gervais et al.[55]
L-phenylalanine HCl	(−)6.08 ± 0.05	0.52 ± 0.03	96 ± 5	129 ± 20	0.26 ± 0.25	91, 13, 10°	this work
glycine HCl	(−)6.42 ± 0.05	0.61 ± 0.03	101 ± 5	100 ± 20	0.30 ± 0.30	95, 0, 0°	this work
glycine HCl	6.5 ± 0.1	0.6 ± 0.1	117 ± 1	[d]	[d]	[d]	Gervais et al.[55]

[a] Chlorine-37 quadrupolar coupling constants were, in all cases, identical within experimental error to $C_Q(^{35}Cl) \times Q(^{37}Cl)/Q(^{35}Cl) = C_Q(^{35}Cl) \times 0.7881$. This is consistent with the findings of Skibsted and Jakobsen.[109] Positive or negative signs given in parentheses are assigned on the basis of quantum chemical calculations. [b] Chemical shifts are reported with respect to solid NaCl at 0 ppm. Isotope effects on the chlorine CS tensor (isotropic and anisotropic part) were assumed to be negligible compared to the precision attainable by these measurements. [c] Euler angles defining the relative orientations of the EFG and CS tensors. Errors are generously estimated as ±20° except for certain more precisely defined cases (see text for further discussion). [d] Not determined. [e] Spectra for L-serine HCl were of poor quality relative to those of the other amino acid hydrochlorides. The data reported here consequently have large errors associated with them and should be considered as preliminary results. [f] Results for L-valine HCl are determined solely from ^{35}Cl and ^{37}Cl NMR spectra of a stationary sample at 11.75 T. Relatively large error limits have consequently been assigned to the chemical shift tensor parameters.

in some cases. The gauge-including atomic orbitals method (GIAO)[97,98] was used for calculating nuclear magnetic shielding tensors.

The EFG and $\boldsymbol{\sigma}$ tensors were diagonalized (after symmetrization in the case of $\boldsymbol{\sigma}$) to obtain the eigenvalues and eigenvectors relating their PAS to the molecular axis system using a C program written specifically for this purpose. The program was also used to generate Minnesota Supercomputer Centre (MSC) "XYZ" (XMol) format files with the tensor PAS represented in the molecular frame. Quadrupolar coupling constants were obtained from V_{33} according to eq 7. The currently accepted values[99] for $Q(^{35}Cl)$ and $Q(^{37}Cl)$ are −81.65 and −64.35 mb, respectively. A factor of 9.7177×10^{21} Vm^{-2} per atomic unit is also required when converting the raw G03 EFG output for use in eq 7.

Conversion of shielding constants to chemical shifts was achieved using the chlorine absolute shielding scale of Gee et al.[69] (eq 4). The following conversion factor was also necessary[54] because some spectra were experimentally referenced to the $^{35/37}Cl$ resonances of solid powdered sodium chloride:

$$\delta(\text{wrt infinitely dilute NaCl(aq)}) = \delta(\text{wrt NaCl(s)}) - 45.37 \text{ ppm} \quad (11)$$

Results and Discussion

(i) Solid-State NMR Spectroscopy. Shown in Table 1 are the chlorine EFG and chemical shift tensor results obtained through spectral simulations of ^{35}Cl and ^{37}Cl NMR spectra of amino acid hydrochlorides important to chloride ion channel selectivity. An inspection of these data, along with our previous results for L-tyrosine HCl,[54] shows that the value of the ^{35}Cl quadrupolar coupling constant ranges from a low of ±2.03 MHz for DL-arginine hydrochloride monohydrate to a maximum of ±6.42 MHz for glycine HCl. Values of $C_Q(^{35}Cl)$ for chloride ions range from essentially zero in cubic salts such as alkali metal chlorides[100,101] to about 1 MHz in alkylammonium chlorides[56,57] to 9.4 MHz in $AlCl_3$.[102] The considerable variation in C_Q for the amino acid hydrochlorides attests to the sensitivity of the ^{35}Cl NMR experiment to the local environment of the chloride anion even within this class of closely related compounds. The quadrupolar asymmetry parameter also shows considerable variation, from 0.25 for L-isoleucine HCl to 0.98 for DL-arginine hydrochloride monohydrate. In several cases, it was possible to experimentally determine the relative orientations of the chlorine EFG and CS tensor principal axis systems; these orientations are depicted alongside the experimental spectra (vide infra).

Shown in Figure 2 are ^{35}Cl and ^{37}Cl SSNMR spectra of L-phenylalanine hydrochloride obtained at 11.75 and 21.15 T. As is the case for many of the HCl salts studied herein, the anisotropic broadening of the CT due to the second-order quadrupolar interaction and chemical shift anisotropy (CSA) is too large (150 kHz or 3061 ppm) at 11.75 T to enable MAS which would provide resolution of spinning sidebands from the centerband. Therefore, our strategy for the precise and accurate determination of the relevant quadrupolar and CS tensor parameters relies on obtaining spectra of stationary samples for both spin-active chlorine isotopes at two applied magnetic fields. Simulation of the lower-field spectra depends less precisely on the magnitude and orientation of the CS tensor relative to the EFG tensor than does that of spectra acquired at higher fields.

The ^{35}Cl quadrupolar coupling constant obtained for L-Phe HCl is 6.08 MHz, and the asymmetry parameter is 0.52. The breadth of the CT powder pattern at 21.15 T, 88 kHz or 998 ppm, indicates immediately the presence of contributions to the spectrum from anisotropy of the CS tensor. If the CT broadening were purely due to the quadrupolar interaction, we would anticipate a scaling of the breadth by 11.75/21.15 T = 55.5% (in Hz) or 30.9% (in ppm) (cf. eq 10). In fact, we observe scalings of 58.7 and 32.6%. The spectra obtained at 21.15 T for L-Phe HCl cannot be fit using an isotropic chlorine CS tensor. This is most strikingly displayed in Figure 2e,f where a well-resolved splitting of the low-frequency edge of the powder

(93) Dunning, T. H., Jr. *J. Chem. Phys.* **1989**, *90*, 1007−1023.
(94) Woon, D. E.; Dunning, T. H., Jr. *J. Chem. Phys.* **1995**, *103*, 4572−4585.
(95) Chesnut, D. B.; Moore, K. D. *J. Comput. Chem.* **1989**, *10*, 648−659.
(96) Chesnut, D. B.; Rusiloski, B. E.; Moore, K. D.; Egolf, D. A. *J. Comput. Chem.* **1993**, *14*, 1364−1375.
(97) Ditchfield, R. *Mol. Phys.* **1974**, *27*, 789−807.
(98) Wolinski, K.; Hinton, J. F.; Pulay, P. *J. Am. Chem. Soc.* **1990**, *112*, 8251−8260.
(99) Pyykkö, P. *Mol. Phys.* **2001**, *99*, 1617−1629.
(100) Weeding, T. L.; Veeman, W. S. *J. Chem. Soc., Chem. Commun.* **1989**, 946−948.
(101) Hayashi, S.; Hayamizu, K. *Bull. Chem. Soc. Jpn.* **1990**, *63*, 913−919.
(102) Sandland, T. O.; Du, L. S.; Stebbins, J. F.; Webster, J. D. *Geochim. Cosmochim. Acta* **2004**, *68*, 5059−5069.

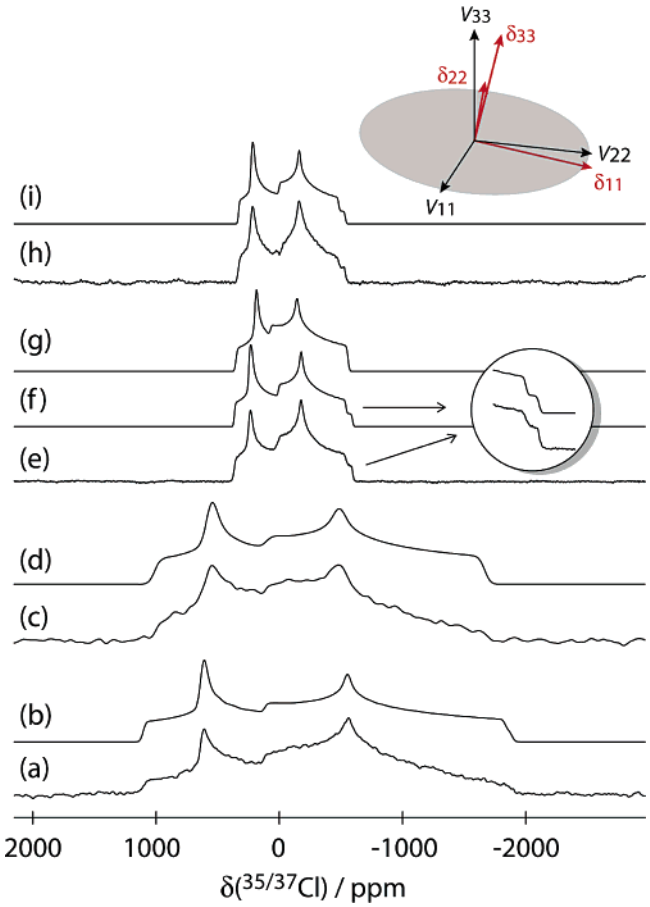

Figure 2. Solid-state chlorine NMR spectroscopy of L-phenylalanine hydrochloride. Experimental spectra of a stationary powdered sample are shown in (a) ^{35}Cl at 11.75 T, (c) ^{37}Cl at 11.75 T, (e) ^{35}Cl at 21.15 T, and (h) ^{37}Cl at 21.15 T. A hyperbolic secant spin−echo sequence was used to acquire the spectra at 11.75 T, and a single pulse was used at 21.15 T. Best-fit spectra, which were simulated using the EFG and CS tensor parameters given in Table 1, are shown in (b), (d), (f), and (i). The effects of an anisotropic chemical shift tensor are clearly evident in the spectra obtained at 21.15 T; shown in trace (g) is the simulated spectrum obtained under the assumption of an isotropic CS tensor. Shown in the inset is the most striking and clear-cut spectral feature which arises because of chemical shift anisotropy; the splitting is 54 ppm and is absent in trace (g). The relative orientations of the chlorine EFG and CS tensor principal axis systems which provided the best-fit simulated spectra are also depicted.

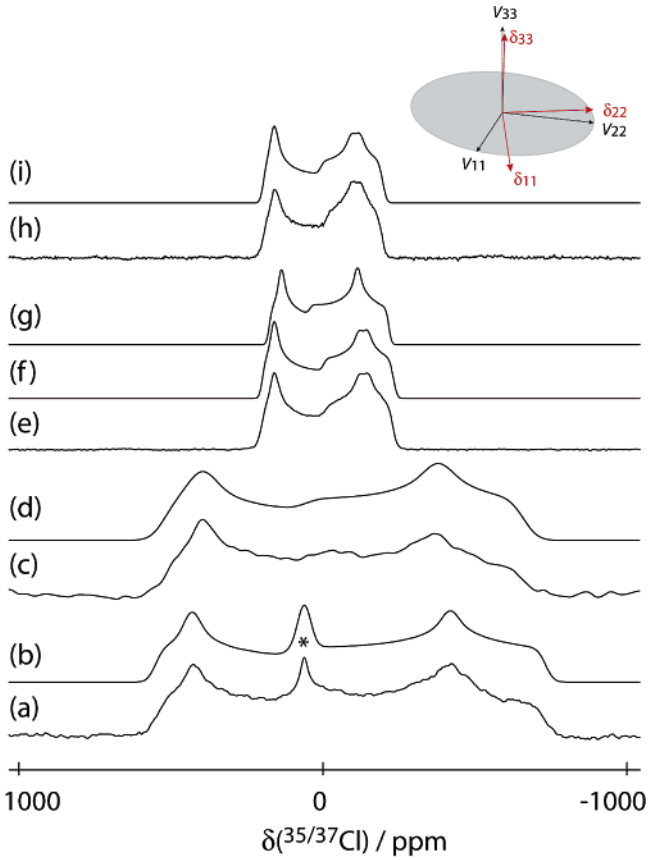

Figure 3. Solid-state chlorine NMR spectroscopy of L-isoleucine hydrochloride. Experimental spectra of a stationary powdered sample are shown in (a) ^{35}Cl at 11.75 T, (c) ^{37}Cl at 11.75 T, (e) ^{35}Cl at 21.15 T, and (h) ^{37}Cl at 21.15 T. A hyperbolic secant spin−echo sequence was used to acquire the spectra at 11.75 T, and a single pulse was used at 21.15 T. Best-fit spectra, which were simulated using the EFG and CS tensor parameters given in Table 1, are shown in (b), (d), (f), and (i). The effects of an anisotropic chemical shift tensor are clearly evident in the spectra obtained at 21.15 T; shown in trace (g) is the simulated spectrum obtained under the assumption of an isotropic CS tensor. A sharp peak at 59.5 ppm due to a solvated component (indicated with an asterisk) was also included in the simulation for ^{35}Cl at 11.75 T; this interpretation is supported by the fact that this solvated component is missing from the remaining spectra, which were recorded a few weeks later. The relative orientations of the chlorine EFG and CS tensor principal axis systems which provided the best-fit simulated spectra are depicted in the inset.

pattern is observed. For comparison, shown in Figure 2g is the simulated spectrum based on the same quadrupolar parameters as those used in Figure 2f but with a CS tensor span of zero.

The quadrupole moment of ^{37}Cl is 78.8% of that of ^{35}Cl,[99] thereby decreasing the influence of the quadrupolar interaction on the CT spectrum of ^{37}Cl relative to that of ^{35}Cl. In principle, the ^{37}Cl NMR spectrum should be more sensitive to chemical shift anisotropy because to a first approximation the CS tensor will be independent of the chlorine isotope we are examining.[103] The splitting due to CSA is also clearly visible in the ^{37}Cl SSNMR spectrum of L-Phe HCl (Figure 2h,i). The CS tensor span obtained from the simulations, 129 ± 20 ppm, is one of the largest reported for chlorine. Hou et al. reported a chlorine CS tensor span of 161 ppm for a dried sample of $LiAl_2(OH)_6$-$Cl{\cdot}nH_2O$.[104] The sensitivity of the simulated spectra of L-Phe HCl to the EFG and CS tensor parameters is presented as Supporting Information.

Shown in Figure 3 are the $^{35/37}$Cl SSNMR spectra of L-isoleucine hydrochloride. The spectral simulations reveal a marked difference between the values of η_Q for L-Ile HCl and L-Phe HCl. Again, at high field, there is a unique spectral feature (a splitting of one of the discontinuities of the powder pattern) which arises due to the presence of the anisotropic chlorine chemical shift (Figure 3e,h) and cannot be simulated by considering solely the quadrupolar interaction (Figure 3g). The value of C_Q(^{35}Cl), 4.39 MHz, is intermediate relative to the range of values reported in Table 1. The CS tensor span, 75 ppm, is significantly different from that obtained for L-Phe HCl, which is interesting as it suggests that the chlorine CS tensor provides additional distinct information on the chlorine environment.

The $^{35/37}$Cl NMR spectra obtained for solid powdered glycine hydrochloride are presented in Figure 4 along with the best-fit spectral simulations. This compound has the largest chlorine

(103) Jameson, C. J. In *Encyclopedia of Nuclear Magnetic Resonance*; Grant, D. M., Harris, R. K., Eds.; Wiley: Chichester, 1996; p 2638.

(104) Hou, X.; Kalinichev, A. G.; Kirkpatrick, R. J. *Chem. Mater.* **2002**, *14*, 2078−2085.

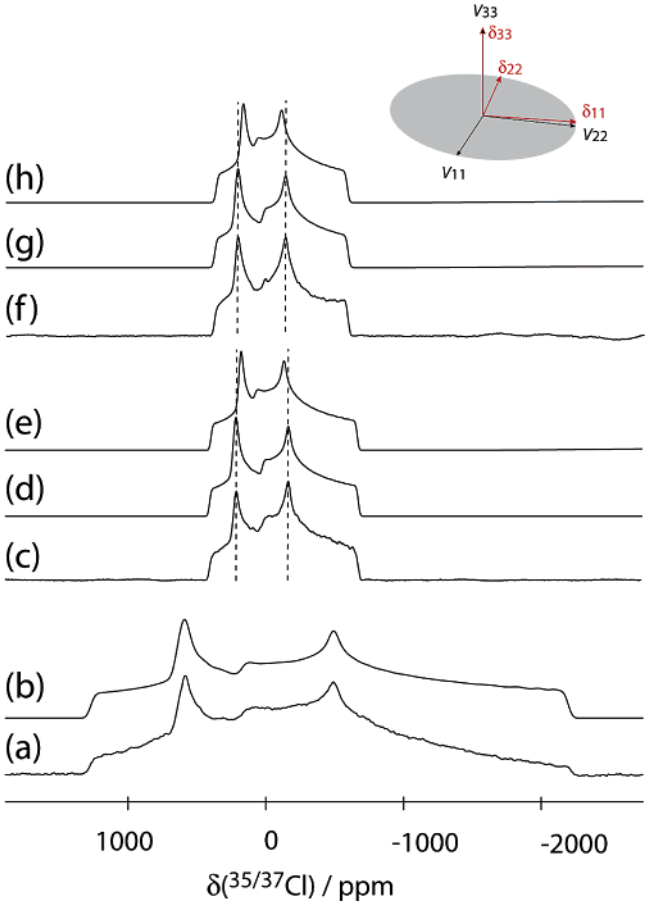

Figure 4. Solid-state chlorine NMR spectroscopy of glycine hydrochloride. Experimental spectra of a stationary powdered sample are shown in (a) ^{35}Cl at 11.75 T, (c) ^{35}Cl at 21.15 T, and (f) ^{37}Cl at 21.15 T. A hyperbolic secant spin−echo sequence was used to acquire the spectra at 11.75 T, and a single pulse was used at 21.15 T. Best-fit spectra, which were simulated using the EFG and CS tensor parameters given in Table 1, are shown in (b), (d), and (g). The effects of an anisotropic chemical shift tensor are clearly evident in the spectra obtained at 21.15 T; shown in traces (e) and (h) are the simulated spectra obtained under the assumption of an isotropic CS tensor. The relative orientations of the chlorine EFG and CS tensor principal axis systems which provided the best-fit simulated spectra are depicted in the inset.

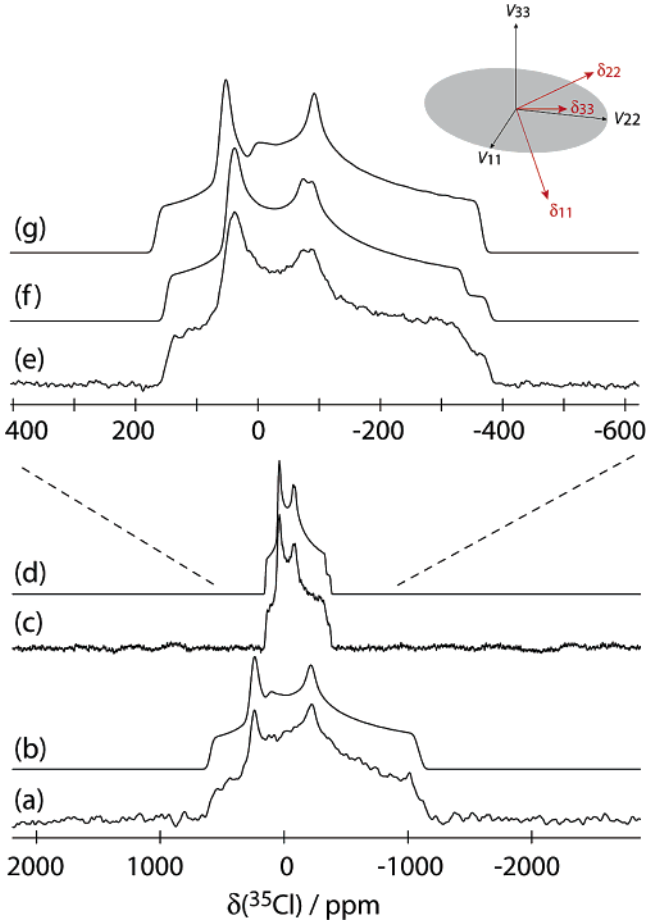

Figure 5. Solid-state chlorine NMR spectroscopy of L-proline hydrochloride. Experimental spectra of a stationary powdered sample are shown in: (a) ^{35}Cl at 11.75 T, (c,e) ^{35}Cl at 21.15 T. A hyperbolic secant spin−echo sequence was used to acquire the spectra at 11.75 T, and a single pulse was used at 21.15 T. Best-fit spectra, which were simulated using the EFG and CS tensor parameters given in Table 1, are shown in (b), (d), and (f). The effects of an anisotropic chemical shift tensor are clearly evident in the spectrum obtained at 21.15 T; shown in trace (g) is the simulated spectrum obtained under the assumption of an isotropic CS tensor. The spectra shown in (e) and (f) are expansions of those shown in (c) and (d). The relative orientations of the chlorine EFG and CS tensor principal axis systems which provided the best-fit simulated spectra are depicted in the inset.

quadrupolar coupling constant reported to date for an amino acid hydrochloride; we obtain a value of 6.42 ± 0.05 MHz. This value is somewhat lower than, but within experimental error of, that reported by Gervais et al., 6.5 ± 0.1 MHz.[55] We attribute the increased precision in our value to the additional NMR data obtained: ^{35}Cl at 11.75 T (Figure 4a); ^{37}Cl at 11.75 T (not shown); ^{35}Cl at 21.15 T (Figure 4c); and ^{37}Cl at 21.15 T (Figure 4f). At 21.15 T, it again becomes clear that the span of the CS tensor is significantly different from zero; in the case of Gly HCl, we find it to be 100 ± 20 ppm. Simulated spectra are particularly sensitive to the Euler angle β, which was precisely characterized as 0° ± 4°.

Spectral results for L-proline hydrochloride are shown in Figure 5. The value of $C_Q(^{35}Cl)$ for L-Pro HCl, 4.50 MHz, is intermediate with respect to those of the other amino acid hydrochlorides. Interestingly, the isotropic chlorine chemical shift, 37 ppm, is anomalous compared to the range obtained for other amino acid hydrochlorides, $\delta_{iso} = 91.5-120$ ppm. The span of the CS tensor is not anomalous, but it is relatively small, $\Omega = 63 \pm 5$ ppm. A similarly small span was also observed for Ile HCl. Simulation of the ^{35}Cl NMR spectrum obtained at 21.15 T (Figure 5e) is very sensitive to β; we find $\beta = 69° \pm 3°$.

Chlorine-35 and chlorine-37 NMR spectra of a stationary sample of solid L-valine hydrochloride are presented, along with the corresponding simulations, as Supporting Information. The value of $C_Q(^{35}Cl)$, 5.89 ± 0.05 MHz, is slightly smaller than that reported previously (6.0 ± 0.1 MHz),[55] as was the case for glycine HCl (vide supra). The present analysis also provides information on the CS tensor (Table 1); we find $\Omega = 125 \pm 40$ ppm.

For all of the HCl salts discussed above, the breadth of the CT powder pattern was broad relative to achievable MAS rates with a 4 mm MAS probe. In the case of L-lysine HCl, ^{35}Cl (Figure 6a) and ^{37}Cl (Figure 6c) MAS NMR spectroscopy yielded ideal second-order quadrupolar line shapes. As expected, the ^{37}Cl MAS NMR spectrum (Figure 6c) exhibits spinning sidebands of reduced intensity at the same MAS rate (14 kHz) due to the lower quadrupole moment of this nucleus. The

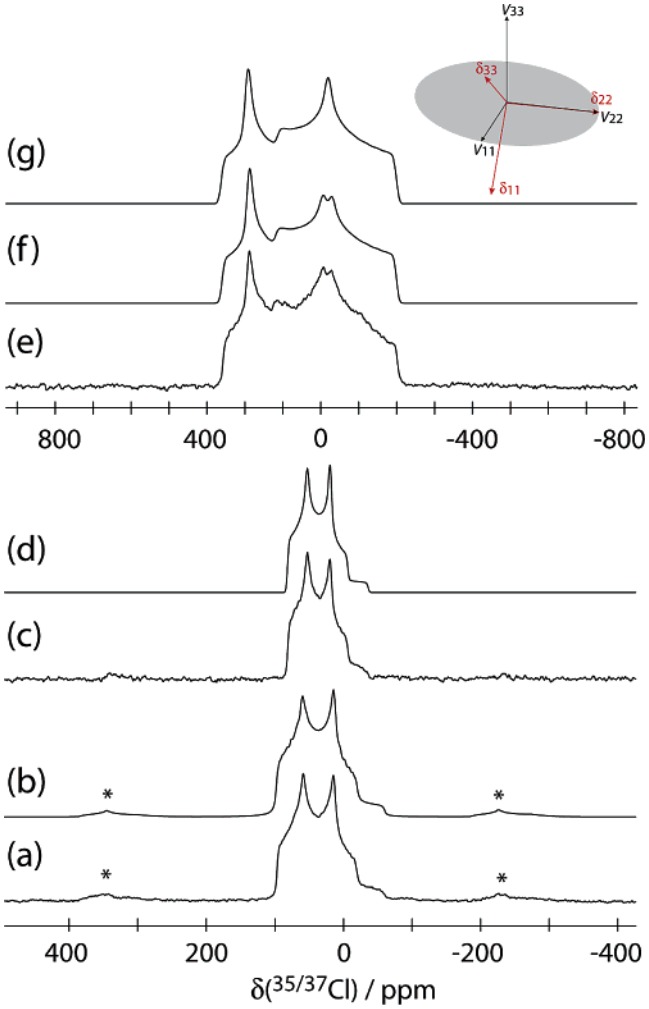

Figure 6. Solid-state chlorine NMR spectroscopy of L-lysine hydrochloride. Experimental spectra of a powdered sample undergoing MAS at a rate of 14 kHz are shown in (a) ^{35}Cl at 11.75 T and (c) ^{37}Cl at 11.75 T. Spinning sidebands are indicated with asterisks. The ^{35}Cl NMR spectrum of a stationary powdered sample obtained at 11.75 T is shown in (e). A hyperbolic secant spin−echo sequence was used to acquire the spectra. Best-fit spectra were simulated using SIMPSON (trace (b)) or WSOLIDS (traces (d) and (f)) using the EFG and CS tensor parameters given in Table 1. The effects of an anisotropic chemical shift tensor are clearly evident in the spectrum of the stationary sample (e); shown in trace (g) is the simulated spectrum obtained under the assumption of an isotropic CS tensor. The relative orientations of the chlorine EFG and CS tensor principal axis systems which provided the best-fit simulated spectra are depicted in the inset.

precision with which δ_{iso}, C_Q, and η_Q are characterized for L-Lys HCl is increased as a result of examining both chlorine isotopes (Table 1). We find $C_Q(^{35}Cl) = 2.49 \pm 0.01$ MHz, and as is the case for all data reported in Table 1, the corresponding independently determined value of $C_Q(^{37}Cl)$ was found to be in keeping with the value predicted from $C_Q(^{35}Cl)$ and the ratio of the quadrupole moments of the nuclei, $2.49 \times (Q(^{37}Cl))/(Q(^{35}Cl)) = 2.49 \times 0.7881 = 1.96$ MHz. An interesting spectrum of a stationary sample was obtained at 11.75 T for L-Lys HCl (Figure 6e). Because of the relatively small value of C_Q in this compound, the effects of chlorine CSA are striking even at this moderate field strength. The key spectral feature, a splitting of one of the discontinuities, cannot be simulated in the absence of CSA. The measured span, 26 ± 10 ppm, is the smallest to be measured precisely for the amino acid hydrochlorides (Table 1).

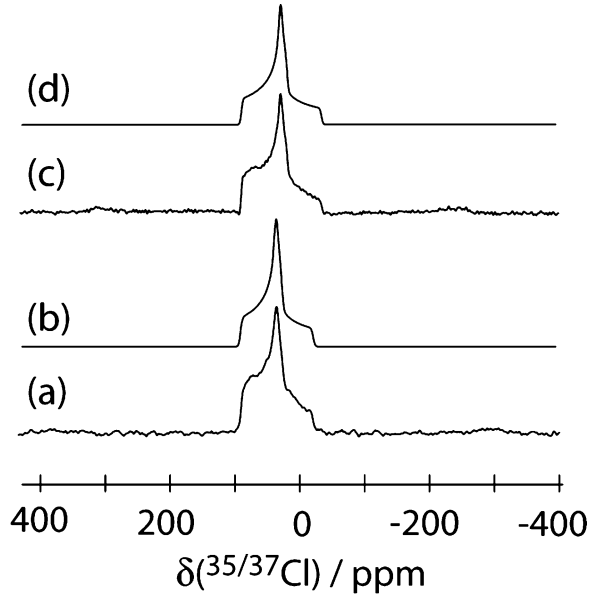

Figure 7. Solid-state chlorine MAS NMR spectroscopy of DL-arginine hydrochloride monohydrate. Experimental spectra of a powdered sample undergoing MAS at a rate of 14 kHz are shown in (a) ^{37}Cl at 11.75 T and (c) ^{35}Cl at 11.75 T. Best-fit spectra were simulated using WSOLIDS (traces (b) and (d)) using the parameters given in Table 1.

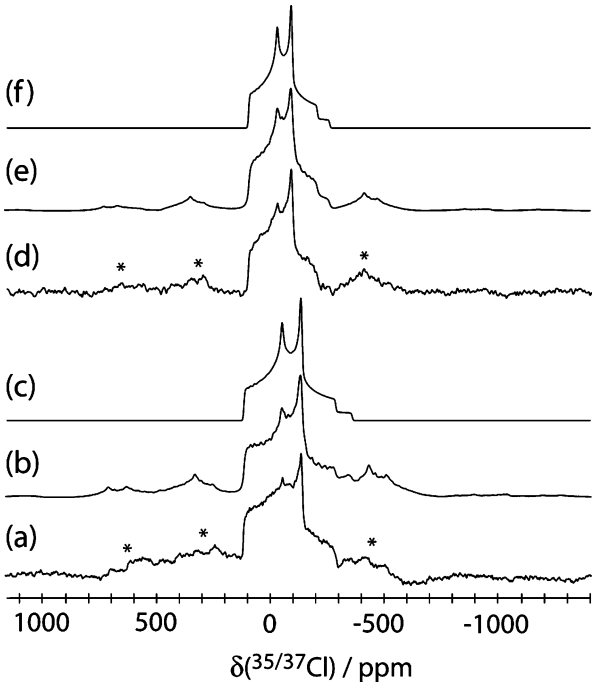

Figure 8. Solid-state chlorine MAS NMR spectroscopy of L-glutamic acid hydrochloride. Experimental spectra of a powdered sample undergoing MAS at a rate of 14 kHz are shown in (a) ^{35}Cl at 11.75 T and (d) ^{37}Cl at 11.75 T. Best-fit spectra were simulated using SIMPSON (traces (b) and (e)) or WSOLIDS (traces (c) and (f)) using the parameters given in Table 1. Spinning sidebands are indicated with asterisks.

The smallest value of $C_Q(^{35}Cl)$ to be observed for an amino acid hydrochloride is 2.03 MHz ($C_Q(^{37}Cl) = 1.60$ MHz) for DL-arginine HCl monohydrate. Chlorine-35/37 MAS NMR at 11.75 T was therefore feasible (Figure 7). Spectral simulations of the MAS NMR spectra (parts b and d) were performed assuming only a single unique chlorine site in the unit cell. However, it is known that there are two crystallographically distinct sites according to the X-ray crystal structure of L-Arg

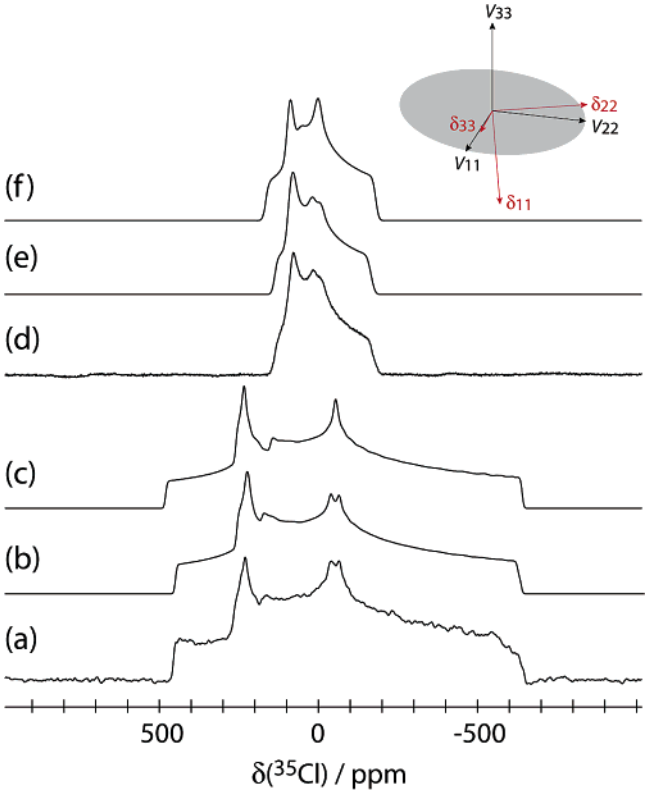

Figure 9. Solid-state chlorine NMR spectroscopy of L-glutamic acid hydrochloride. Experimental spectra of a stationary powdered sample are shown in (a) ^{35}Cl at 11.75 T and (d) ^{35}Cl at 21.15 T. A hyperbolic secant spin−echo sequence was used to acquire the spectrum at 11.75 T, and a single pulse was used at 21.15 T. Best-fit spectra, which were simulated using the EFG and CS tensor parameters given in Table 1, are shown in (b) and (e). The effects of an anisotropic chemical shift tensor are clearly evident; shown in traces (c) and (f) are the simulated spectra obtained under the assumption of an isotropic CS tensor. The relative orientations of the chlorine EFG and CS tensor principal axis systems which provided the best-fit simulated spectra are depicted in the inset.

HCl H_2O.[105] Efforts to resolve the two sites by ^{35}Cl satellite-transition NMR spectroscopy (SATRAS[106−108]) were not successful, which is not surprising considering the details of the X-ray structure. The differences between the two arginine moieties in the unit cell are exceedingly small. The standard deviation between the bond lengths involving heavy atoms for the two moieties is only 0.0037 Å, and the standard deviation of the angles is only 0.57°. Evidently, such small differences do not manifest themselves in a measurable way in the chlorine EFG tensor in a magnetic field of 11.75 T.

Glu148 is a critical amino acid residue in the ion conduction pathway of the ClC ion channels; its carboxylate side chain interacts through a hydrogen bond with the chloride ions in the channel,[16] as is also the case in the neutron diffraction structure of L-glutamic acid hydrochloride (cf. Figure 1).[88] Shown in Figure 8 are the ^{35}Cl and ^{37}Cl MAS NMR spectra of L-Glu HCl obtained at 11.75 T. The values determined here, $C_Q(^{35}Cl) = 3.61 \pm 0.01$ MHz, $\eta_Q = 0.65 \pm 0.02$, and $\delta_{iso} = 102 \pm 1$ ppm, are close to those reported previously,[55] 3.7 ± 0.1 MHz, 0.6 ± 0.1, and 104 ± 1 ppm. Spectra of a stationary sample of L-Glu

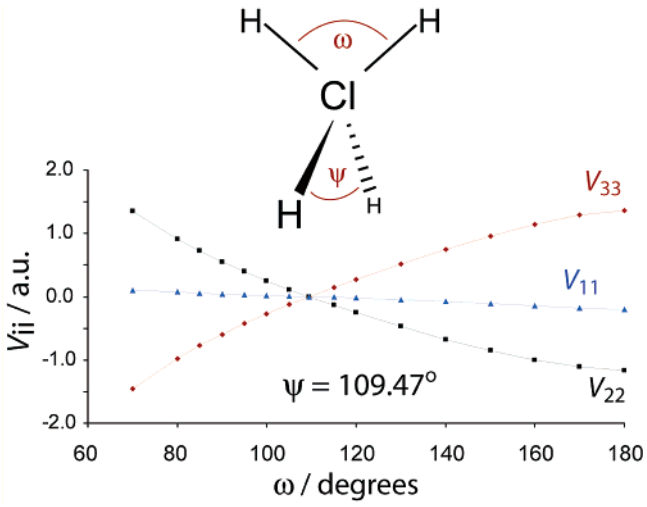

Figure 10. Distorted tetrahedron/seesaw model, consisting of a ClH_4^{3+} moiety, for assessing the dependence of the EFG tensor on local geometry, characterized by two angles, ω and ψ. Shown in the plot are the results of B3LYP/3-21G* calculations of the chlorine EFG tensor for various values of ω while ψ is fixed at the tetrahedral angle. Note the sensitivity of the magnitude and sign of V_{33}, as well as the value of η_Q, to ω when $\omega \sim 109.47°$. Additional calculations using this model are given as Supporting Information.

HCl afforded the novel opportunity to characterize the chlorine CS tensor (Figure 9). Even at 11.75 T, a distinct spectral splitting clearly indicates the presence of significant chlorine CSA, with $\Omega = 66 \pm 15$ ppm (Figure 9a). L-Glu HCl offers an interesting example of chemical shift anisotropy which decreases, rather than increases, the breadth of the CT powder pattern relative to that expected for purely quadrupolar broadening. The simulated spectra presented in Figure 9c,f are based purely on the quadrupolar interaction and are broader than the best-fit spectra presented in Figure 9b,e. In the present case, this effect may be attributed to the β angle (77°), which approaches 90°.

In all of the analyses discussed above, we have assumed that isotope effects[103] on the chlorine CS tensor are negligible. Given the precision attainable, particularly in the analysis of stationary samples, this is an acceptable approximation. Skibsted and Jakobsen have previously examined ^{35}Cl and ^{37}Cl MAS NMR spectra of several perchlorate salts and found $\delta_{iso}(^{35}Cl)$ and $\delta_{iso}(^{37}Cl)$ to be identical within experimental error (0.3−0.5 ppm) in all cases.[109]

(ii) Interpretation of Chlorine Electric Field Gradient and Chemical Shift Tensors. (a) Distorted Tetrahedron/Seesaw Model. A previously proposed model for the interpretation of the trend in $C_Q(^{35}Cl)$ for organic hydrochloride salts suggested that the number of hydrogen bonds to Cl was a dominant factor.[54] The new data acquired in the present study are consistent with this model; however, it is apparent that, once three or four hydrogen bonds are present, other factors become important in determining the precise value of C_Q within closely related amino acid hydrochloride salts.

In four of the five structures shown in Figure 1, the chloride ion is coordinated by four hydrogen bonds arranged in a distorted tetrahedral geometry. If all four substituents were equivalent and were arranged in a perfect tetrahedron, the principal components of the EFG tensor would be identically zero. In a very simple model, we can consider the distortion of

(105) Dow, J.; Jensen, L. H.; Mazumdar, S. K.; Srinivasan, R.; Ramachandran, G. N. *Acta Crystallogr.* **1970**, *B26*, 1662−1671.
(106) Samoson, A. *Chem. Phys. Lett.* **1985**, *119*, 29−32.
(107) Jäger, C. *NMR Basic Princ. Prog.* **1994**, *31*, 133−170.
(108) Skibsted, J.; Nielsen N. C.; Bildsøe, H.; Jakobsen, H. J. *J. Magn. Reson.* **1991**, *95*, 88−117.
(109) Skibsted, J.; Jakobsen, H. J. *Inorg. Chem.* **1999**, *38*, 1806−1813.

Table 2. Calculated Chlorine Quadrupolar and Magnetic Shielding Tensors for L-Phenylalanine Hydrochloride

method	basis set[a]	$C_Q(^{35}Cl)$/MHz	η_Q	σ_{11}/ppm	σ_{22}/ppm	σ_{33}/ppm	σ_{iso}/ppm	δ_{iso}[b]/ppm	Ω/ppm	κ
B3LYP	6-31G*/3-21G	−7.68	0.60	907.6	957.4	1020.9	961.9	57.5	113.3	0.12
B3LYP	6-311+G*/3-21G	−7.62	0.71	901.6	949.9	1002.1	951.2	68.2	100.5	0.04
B3LYP	6-311+G*/6-31G	−7.83	0.70	893.2	940.3	1000.0	944.5	74.9	106.8	0.12
B3LYP	6-311++G**	−7.75	0.72	844.5	895.7	980.8	907.0	112.4	136.3	0.25
B3LYP	cc-pVDZ	−7.24	0.68	896.8	946.7	1017.5	953.7	65.7	120.7	0.17
B3LYP	aug-cc-pVDZ/cc-pVDZ	−6.81	0.73	878.5	931.4	998.2	936.0	83.4	119.7	0.12
B3LYP	cc-pVTZ/cc-pVDZ	−8.16	0.71	909.4	955.9	1020.5	961.9	57.5	111.1	0.16
RHF	6-311+G*	−5.53	0.73	941.2	974.8	1042.4	986.1	33.3	101.2	0.33
RHF	6-311++G**	−5.67	0.73	940.0	970.5	1042.6	984.4	35.0	102.6	0.41
RHF	cc-pVDZ	−4.84	0.71	953.9	987.5	1056.8	999.4	20.0	102.9	0.35
RHF	aug-cc-pVDZ/cc-pVDZ	−4.63	0.76	946.6	982.0	1044.7	991.1	28.3	98.1	0.28
RHF	cc-pVTZ/cc-pVDZ	−5.93	0.74	977.7	1006.7	1066.4	1016.9	2.5	88.7	0.34
PBEPBE	6-311+G*	−8.30	0.70	824.7	888.6	968.5	893.9	125.5	143.8	0.11
PBEPBE	6-311++G**	−8.37	0.69	819.4	878.8	964.0	887.4	132.0	144.6	0.18
PBEPBE	aug-cc-pVDZ/cc-pVDZ	−7.72	0.71	857.1	915.9	981.6	918.2	101.2	124.5	0.06
exptl		$\pm\lvert 6.08 \pm 0.05\rvert$	0.52 ± 0.03					96 ± 5	129 ± 20	0.26 ± 0.25

[a] The notation, e.g., cc-pVTZ/cc-pVDZ, indicates that the cc-pVTZ basis set was used on chlorine and the cc-pVDZ basis set was used on all other atoms. [b] Chemical shifts are reported with respect to solid NaCl at 0 ppm.

a tetrahedron toward a "seesaw" structure, with two variable angles (Figure 10). Fixing one angle, ψ, at 109.47° and varying the second angle, ω, from 70 to 180° yields an interesting result: when ω is close to the tetrahedral angle, the sign of V_{33}, and hence the sign of C_Q, is very sensitive to the precise value of ω. This observation suggests that the experimentally measured values of $C_Q(^{35}Cl)$ need not all be the same sign (see Supporting Information for additional calculations). Indeed, previous work[54] has indicated that $C_Q(^{35}Cl)$ is positive for L-Tyr HCl, yet all calculated values of $C_Q(^{35}Cl)$ for L-Phe HCl in the present work are negative (vide infra, Table 2). The value of η_Q is also very sensitive to ω when ω approaches 109.47°. This simple model provides some interesting insights; however, in trying to predict quadrupolar coupling constants on the basis of only two angles around Cl, there is clearly some ambiguity in which two angles are chosen, and in reality, all four chloride substituents are not equal.

A second, only slightly more sophisticated, model was therefore developed to test whether the trend in experimental chlorine quadrupolar coupling constants could be reproduced. Again, a structure consisting of only a central chloride anion and the protons to which it is hydrogen bonded (using neutron diffraction coordinates for L-Phe HCl, Gly HCl, L-Val HCl, L-Glu HCl, and L-Tyr HCl) was considered. Low-level quantum chemical calculations (B3LYP/3-21G*) were performed on each of these simple ClH_4^{3+} systems, and the results are presented in Figure 11. A positive correlation (Pearson's correlation coefficient, $R = 0.973$) between $|V_{33}|$ and the experimentally determined C_Q values is observed. These results suggest that the positions of the hydrogen-bonded protons dominate the observed trend in chlorine quadrupolar coupling constants, despite the contributions to the EFG from the rest of the electrons in the surrounding crystal lattice (which vary with r^{-3}, where r is the electron−nucleus distance[110]). The success of this simple model is informative; nevertheless, a more quantitative agreement between experiment and theory was pursued and achieved, as described below.

(110) Pound, R. V. *Phys. Rev.* **1950**, *79*, 685−702.

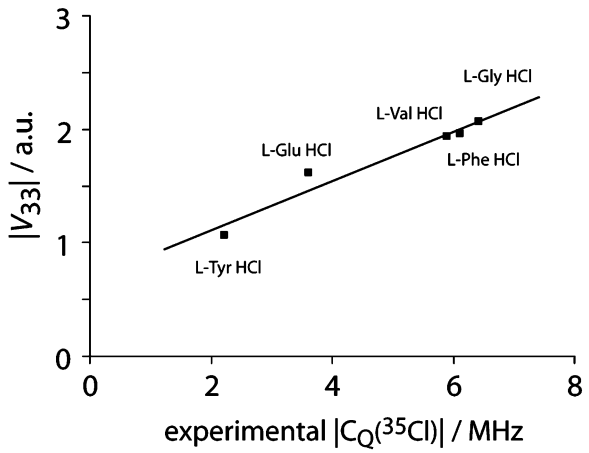

Figure 11. Correlation between the calculated absolute value of the largest component of the electric field gradient (V_{33}) and the absolute value of the experimental ^{35}Cl quadrupolar coupling constant measured in the solid state for various amino acid hydrochlorides. Calculations (B3LYP/3-21G*) were performed for compounds for which neutron diffraction structures are available: glycine HCl, L-tyrosine HCl, L-valine HCl, L-glutamic acid HCl, and L-phenylalanine HCl. The model used in the calculations consisted only of the chloride anion and the protons involved in hydrogen bonds to Cl (ClH_4^{3+}). See text for further discussion. Linear regression yields: $|V_{33}| = 0.2158(|C_Q|) + 0.6655$; $R = 0.973$.

(b) Quantum Chemical Calculations. The experimental NMR results obtained for L-phenylalanine hydrochloride provide precise chlorine CS and EFG tensor measurements for a compound for which there is also a high-quality neutron diffraction structure[85] that provides reliable proton positions. Several quantum chemical calculations of the chlorine NMR interaction tensors for L-Phe HCl were performed to determine an optimum method which would provide reliable quadrupolar coupling constants and CS tensor parameters at moderate computational expense (Table 2). The model used in these calculations, comprising 97 atoms, included four L-phenylalanine cations coordinated to a chloride ion (Figure 1). No quantum chemical geometry optimization was performed prior to the calculation of the NMR interaction tensors; the same geometry was used for each calculation. Calculated ^{35}Cl quadrupolar

Table 3. Calculated Chlorine Quadrupolar and Magnetic Shielding Tensors for Selected Amino Acid Hydrochlorides for Which Neutron Diffraction Structures Are Available

	method	basis set[a]	$C_Q(^{35}Cl)$/MHz	η_Q	σ_{11}/ppm	σ_{22}/ppm	σ_{33}/ppm	σ_{iso}/ppm	δ_{iso}[b]/ppm	Ω/ppm	k
L-valine HCl	RHF	cc-pVTZ/cc-pVDZ	−5.86	0.71	969.7	1017.0	1065.2	1017.3	2.1	95.5	0.01
	B3LYP	aug-cc-pVDZ/cc-pVDZ	−6.82	0.79	874.1	940.0	1001.6	938.6	80.8	127.5	−0.03
L-tyrosine HCl	RHF	cc-pVTZ/cc-pVDZ	2.08	0.29	980.0	1038.2	1059.3	1025.8	−6.4	79.3	−0.47
	B3LYP	aug-cc-pVDZ/cc-pVDZ	2.84	0.49	892.9	949.6	980.2	940.9	78.5	87.3	−0.30
L-glutamic acid HCl	RHF	cc-pVTZ/cc-pVDZ	3.60	0.55	989.3	1000.5	1027.3	1005.7	13.7	38.0	0.41
	B3LYP	aug-cc-pVDZ/cc-pVDZ	4.36	0.74	901.5	923.5	968.0	931.0	88.4	66.5	0.34
glycine HCl	RHF	cc-pVTZ/cc-pVDZ	−6.50	0.67	1001.0	1034.1	1084.5	1039.9	−20.5	83.5	0.21
	B3LYP	aug-cc-pVDZ/cc-pVDZ	−7.48	0.46	906.6	952.0	1009.9	956.2	63.2	103.3	0.12

[a] The notation, e.g., cc-pVTZ/cc-pVDZ, indicates that the cc-pVTZ basis set was used on chlorine and the cc-pVDZ basis set was used on all other atoms. [b] Chemical shifts are reported with respect to solid NaCl at 0 ppm.

coupling constants range from −4.63 MHz at the RHF level with the aug-cc-pVDZ basis set on chlorine and the cc-pVDZ basis set on all other atoms to −8.37 MHz using the PBEPBE DFT method with the 6-311++G** basis set. Although it is reassuring that the experimental value of $C_Q(^{35}Cl) = \pm 6.08$ MHz falls within this range, such a range is unacceptably large. Because the same high-quality neutron diffraction structure is being used for each calculation, the range of observed values reflects only differences in the accuracy of the EFG tensor calculation. Past calculations on similar systems have consistently overestimated experimental values. For example, a calculated value of 8.46 MHz has been reported for glycine HCl[55] (cf. our experimental value of 6.42 ± 0.05 MHz). As shown in Table 2, in general, the RHF method underestimates C_Q and the B3LYP and PBEPBE functionals overestimate C_Q. A basis-set study using the RHF and B3LYP methods was carried out, and in the case of L-Phe HCl, we find that the B3LYP/aug-cc-pVDZ (on Cl)/cc-pVDZ (on all other atoms) calculation and the RHF/cc-pVTZ/cc-pVDZ calculation provide results which approach the experimental value: −6.81 and −5.93 MHz. In particular, the RHF calculation performs impressively and underestimates C_Q by less than 3%. All results suggest that C_Q is negative.

For the remaining HCl salts for which neutron diffraction structures exist, quantum chemical calculations were also performed. The results presented in Table 3 indicate that the RHF/cc-pVTZ/cc-pVDZ calculation, which predicted C_Q with excellent accuracy for L-Phe HCl, also reproduces C_Q for L-Val HCl, Gly HCl, L-Glu HCl, and L-Tyr HCl to within 0.7, 1.2, 0.3, and 6.7%, respectively, corresponding to a root-mean-square deviation of only 0.1 MHz and a Pearson's correlation coefficient, R, of 0.9998 (Figure 12). We conclude that the RHF/cc-pVTZ/cc-pVDZ method is well suited to the calculation of chlorine quadrupolar coupling constants in organic hydrochlorides. In the case of L-Glu HCl, agreement between experiment and theory was obtained only upon inclusion of two glutamic acid moieties in which methylene protons are found at distances of 3.0 and 3.1 Å from the chloride ion (see Figure 1d).

The experimental CS tensor span for L-Phe HCl, 129 ± 20 ppm, is well reproduced by the B3LYP calculations (100.5−136.3 ppm) as well as by the PBEPBE/aug-cc-pVDZ/cc-pVDZ calculation (124.5 ppm). However, all RHF results consistently underestimate this experimental value (Table 2). All calculations predict a positive skew and provide values which are in agreement with the experimental range of 0.3 ± 0.2. The chlorine isotropic chemical shift for L-Phe HCl (110 ± 5 ppm) is not well reproduced by the calculations (except, perhaps fortuitously, by the B3LYP/6-311++G** calculation, which gives 112.4 ppm). This fact emphasizes the importance of characterizing the CS tensor properties rather than simply the isotropic chemical shift. When B3LYP/aug-cc-pVDZ (on Cl)/cc-pVDZ (on all other atoms) calculations are performed on all four compounds for which neutron diffraction structures exist and for which Ω has been characterized, excellent agreement is obtained as shown in Figure 13. The magnitude of Ω observed for the HCl salts, which is dependent upon the paramagnetic shielding according to Ramsey's theory,[65] represents only a small fraction of the total known chlorine chemical shift range (on the order of 1000 ppm).[111,112] The relative and absolute

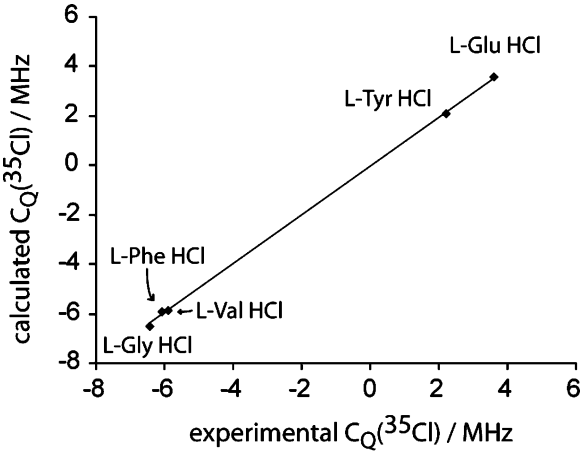

Figure 12. Correlation between chlorine-35 quadrupolar coupling constants calculated at the RHF/cc-pVTZ/cc-pVDZ level and those measured by chlorine solid-state NMR spectroscopy for the following amino acid hydrochlorides: L-Gly HCl, L-Phe HCl, L-Val HCl, L-Tyr HCl, and L-Glu HCl. Linear regression yields: $C_Q(\text{calcd}) = 0.9886 \times C_Q(\text{exptl}) - 0.0386$ and $R = 0.9998$. The rms deviation of the fit is 0.1 MHz.

(111) Lindman, B.; Forsén, S. *NMR Basic Princ. Prog.* **1976**, *12*, 1−365.
(112) Lindman, B.; Forsén, S. In *NMR and the Periodic Table*; Harris, R. K., Mann, B. E., Eds.; Academic Press: London, 1978; Chapter 13.

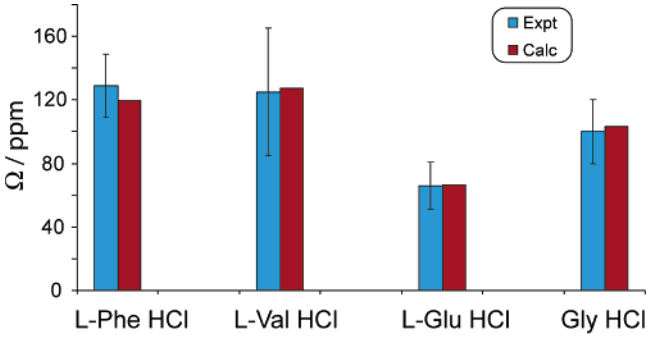

Figure 13. Comparison between experimental (blue) and calculated (red) chlorine chemical shift tensor spans for L-phenylalanine hydrochloride, L-valine hydrochloride, L-glutamic acid hydrochloride, and glycine hydrochloride. Calculations were carried out at the B3LYP level, with the aug-cc-pVDZ basis set on Cl and the cc-pVDZ basis set on all other atoms. Models used in the calculations are shown in Figure 1.

chlorine EFG and CS tensor orientations determined from the RHF/cc-pVTZ/cc-pVDZ calculations are presented as Supporting Information. For L-Val HCl, Gly HCl, L-Phe HCl, and L-Tyr HCl, the calculated chlorine tensors are oriented such that V_{33} and σ_{11} are approximately directed along one of the Cl···H−N hydrogen bonds. For L-Gly HCl, σ_{11} is oriented along one of these bonds as well.

To assess the sensitivity of the calculations of C_Q in L-Phe HCl to the positions of the protons which surround the chloride ion, these positions were optimized at the RHF/3-21G* level while the heavy atoms remained fixed. A subsequent calculation of $C_Q(^{35}Cl)$ at the RHF/cc-pVTZ/cc-pVDZ level on the optimized structure resulted in −5.07 MHz, a reduction of 15% relative to the value obtained without optimization (and also a 15% reduction relative to the experimental value). This result speaks to the accuracy with which the proton positions must be known for reliable calculated results to be obtained. Additional calculated results are presented as Supporting Information for L-proline HCl using heavy-atom atomic coordinates from the X-ray structure[113] and quantum chemical optimization of the proton coordinates. Not surprisingly, the calculated values of C_Q deviate from the experimental values by several percent. For L-Pro HCl, in which chloride ions are separated by only 4.6 Å, improvements in the quantitative accuracy of the calculated quadrupolar parameters may be possible using the self-consistent charge field perturbation approach (SC−CFP) described by Zhang et al.[114]

(c) ClC Channel. To evaluate the magnitudes of chlorine EFG and CS tensors in the ClC channel (PDB entry 1KPL), quantum chemical calculations using the optimum methods and basis sets described above were performed on the model system shown in Figure 14. The chloride ion is coordinated to four traditional hydrogen-bond donors: a side chain OH group from Tyr445, a side chain OH group from Ser 107, and backbone NH groups Ile356 and Phe357. There are additional close contacts to the methylene protons of Gly355 and Phe357. The results obtained for the quadrupolar parameters, $C_Q(^{35}Cl) = -2.07$ MHz and $\eta_Q = 0.76$ (RHF/cc-pVTZ/cc-pVDZ), are most similar to those for DL-arginine HCl·H_2O and L-tyrosine HCl. The CS tensor parameters, calculated at the B3LYP/aug-cc-pVDZ/cc-pVDZ level, are $\delta_{iso} = 56.7$ ppm, $\Omega = 59.6$ ppm, and $\kappa = -0.60$. The relatively small magnitudes of the calculated EFG and CS tensor parameters suggest that $^{35/37}$Cl SSNMR studies of ClC channels will not be hindered by impractically broad NMR line shapes.

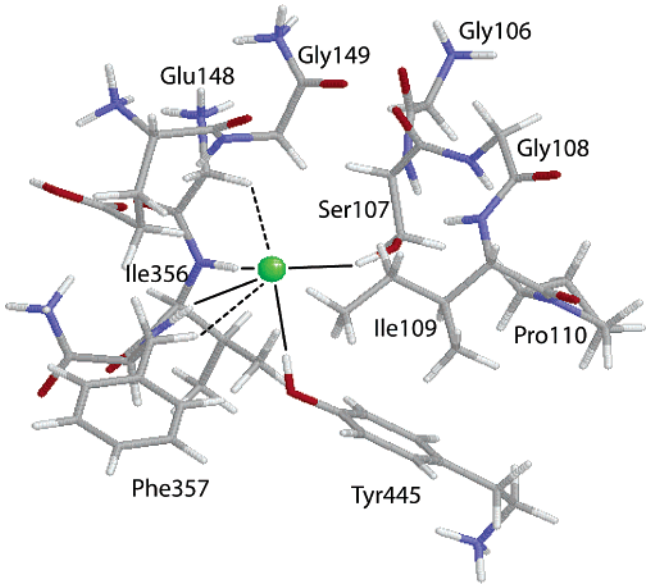

Figure 14. Chloride ion binding site in ClC channels (PDB 1KPL).[16] Some amino acid side chains which are not immediately involved in interactions with Cl^- have been truncated to reduce the computational time required for CS and EFG tensor calculations. Protons have been added and optimized at the B3LYP/3-21G* level. Hydrogen bonds involving chlorine are indicated by solid black lines; two additional close contacts to methylene protons are denoted with dashed lines.

Concluding Remarks

The increasing availability of ultrahigh-field SSNMR spectrometers will undoubtedly continue to render amenable for study more of the quadrupolar nuclei in the periodic table. It has been shown that chlorine-35/37 NMR spectra of solid amino acid hydrochlorides are readily obtainable, and careful interpretation has provided several benchmark chlorine EFG and CS tensor data, thereby greatly increasing the amount of chlorine NMR tensor data available in the literature. In particular, the necessity of considering the effects of anisotropic magnetic shielding in the interpretation of $^{35/37}$Cl NMR spectra of stationary powders at 21.15 T has been demonstrated in several cases. This point is expected to come to bear on the interpretation of SSNMR spectra of any quadrupolar nucleus observed in an ultrahigh-field magnet.

Although it is tempting to try to establish general conclusions regarding simple correlations between the measured chlorine EFG and CS tensors and an easily quantifiable structural parameter, in fact, these tensors depend on many parameters. We have proposed and applied a simple model for rationalizing the observed trend in chlorine quadrupolar coupling constants and found that the experimental trend is reproducible when only the nearest-neighbor hydrogen-bonded protons are considered. Quantitative agreement (rmsd = 0.1 MHz) between experimental and calculated chlorine quadrupolar coupling constants has been achieved for amino acid hydrochlorides, based in part on knowledge of their neutron diffraction structures. This represents a significant improvement over previous attempts to reproduce experimental chlorine quadrupolar coupling constants. Agree-

(113) Mitsui, Y.; Tsuboi, M.; Iitaka, Y. *Acta Crystallogr.* **1969**, *B25*, 2182−2192.
(114) Zhang, Y.; Mukherjee, S.; Oldfield, E. *J. Am. Chem. Soc.* **2005**, *127*, 2370−2371.

ment within experimental error has also been achieved in the calculation of chlorine chemical shift tensor spans. The excellent correspondence between experiment and theory suggests that chlorine EFG and CS tensor data should provide a novel experimental tool for the refinement of structural parameters around chloride ion binding sites in larger ion channel systems.

Interestingly, the larger chlorine quadrupolar coupling constants observed for HCl salts tend to correspond to those amino acids which are considered to be hydrophobic according to the hydropathy index of Kyte and Doolittle,[115] e.g., L-Phe HCl, L-Val HCl, and L-Ile HCl. The smaller C_Q values tend to be associated with HCl salts of hydrophilic amino acids, e.g., DL-Arg HCl·H_2O, L-Lys HCl, L-Ser HCl, and L-Glu HCl. There is no fundamental reason for there to be a correlation between amino acid hydropathy and the chlorine EFG tensor; however, hydrophilic amino acid side chains comprise additional NH or OH groups which are available for hydrogen bonding to chloride, whereas hydrophobic amino acids such as L-Phe HCl must arrange themselves in the solid state to form hydrogen bonds to Cl^- using only the backbone H-bonding sites. We suggest that the greater flexibility in hydrogen-bonding arrangements available to the hydrophilic side chains may allow for an increased number of H bonds to chlorine and perhaps a more symmetrical arrangement of these bonds, resulting in reduced chlorine quadrupolar coupling constants.

The relationships between the chlorine NMR interaction tensors and the local molecular structure established in this work represent a vital step toward the development of solid-state chlorine NMR spectroscopy as a tool for studying larger ion channel systems, for which alternative structural information may be difficult or impossible to obtain.

(115) Kyte, J.; Doolittle, R. F. *J. Mol. Biol.* **1982**, *157*, 105−132.

Acknowledgment. We are grateful to Dr. Glenn Facey and Dr. Victor Terskikh for technical assistance and helpful comments. We thank Prof. Rod Wasylishen, Dr. Renée Siegel, and Dr. Tom Nakashima for providing the pulse code for the hyperbolic secant echo sequence and Rod for helpful discussions. Mr. Jamie Bennett (NRC, Ottawa) is thanked for construction of the NMR probe used at 21.1 T. Access to the 900 MHz NMR spectrometer was provided by the National Ultrahigh-Field NMR Facility for Solids (Ottawa, Canada), a national research facility funded by the Canada Foundation for Innovation, the Ontario Innovation Trust, Recherche Québec, the National Research Council of Canada, and Bruker Biospin and managed by the University of Ottawa (www.nmr900.ca). Thanks to Dr. Klaus Eichele for his excellent software. G03 calculations were carried out using the High Performance Virtual Computing Laboratory. D.L.B. thanks the Natural Sciences and Engineering Research Council (NSERC) of Canada and the University of Ottawa Faculty of Science for generous funding. G.D.S. is grateful to the Canadian Summer Career Placements program for funding, and S.A. thanks NSERC for an Undergraduate Student Research Award.

Supporting Information Available: Figures showing the following: sensitivity of spectral fits to the CS and EFG tensor parameters, experimental results for L-valine hydrochloride, additional computational results for the seesaw model, various models used in calculations on L-proline hydrochloride, and calculated EFG and CS tensor orientations. Tables summarizing the following: calculated results for L-proline hydrochloride and the calculated Euler angles for five HCl salts. Full details for refs 6, 7, and 84. This material is available free of charge via the Internet at http://pubs.acs.org.

JA057253I